NOAA Technical Memorandum ERL ARL-154

SHORT-TERM TEMPORAL VARIATIONS OF NIMBUS-7 MEASUREMENTS OF THE SOLAR UV SPECTRAL IRRADIANCE

Richard F. Donnelly
David E. Stevens
Joan Barrett
Karl Pfendt

Air Resources Laboratory
Silver Spring, Maryland
June 1987

noaa NATIONAL OCEANIC AND ATMOSPHERIC ADMINISTRATION / Environmental Research Laboratories

NOAA Technical Memorandum ERL ARL-154

SHORT-TERM TEMPORAL VARIATIONS OF NIMBUS-7 MEASUREMENTS OF THE SOLAR UV SPECTRAL IRRADIANCE

Richard F. Donnelly
David E. Stevens
Joan Barrett
Karl Pfendt

Sun-Climate Staff
Boulder, Colorado

Air Resources Laboratory
Silver Spring, Maryland
June 1987

UNITED STATES
DEPARTMENT OF COMMERCE

Malcolm Baldrige,
Secretary

NATIONAL OCEANIC AND
ATMOSPHERIC ADMINISTRATION

Anthony J. Calio,
Administrator

Environmental Research
Laboratories

Vernon E. Derr,
Director

NOTICE

Mention of a commercial company or product does not constitute an endorsement by NOAA Environmental Research Laboratories. Use for publicity or advertising purposes of information from this publication concerning proprietary products or the tests of such products is not authorized.

For sale by the National Technical Information Service, 5285 Port Royal Road
Springfield, VA 22161

TABLE OF CONTENTS

Short-Term Temporal Variations of NIMBUS-7 Measurements of the Solar UV Spectral Irradiance

Richard F. Donnelly, David E. Stevens, Joan Barrett and Karl Pfendt
Sun-Climate Staff, Air Resources Laboratory, NOAA ERL
Boulder, Colorado 80303

ABSTRACT

NIMBUS-7 measurements of the solar spectral irradiance in the 160-400 nm range during November 7, 1978 - October 29, 1984, were analyzed to determine the characteristics of their short-term variations (days and weeks to a couple of months). The persistence of solar-rotational variations is shown to be uniformly high for the UV wavelengths important for inducing stratospheric photochemical reactions and for heating the stratosphere, which contrasts greatly with the low and nonuniform persistence for coronal EUV wavelengths and the standard ground-based measures of solar variability, the Ottawa 10.7 cm flux (F10) and sunspot number (R). The persistence of Heath's UV index, the Mg II h & k line center-to-wing ratio, which is insensitive to instrumentation drifts and therefore a good measure of long-term UV variations, agrees well with the persistence of the Mg II center flux, the Mg I line at 285 nm and the UV flux in the 170 - 260 nm range. The persistence of the Al I edge ratio is usually lower than for UV fluxes in the 170 - 260 nm range because of the reduced signal to noise ratio in the edge ratio.

Periodicity in the 13 - 14 day range is the second strongest short-term variation (27 - 28 day solar rotational variations are the strongest short-term periodicity). The 13-day periodicity is fairly strong relative to that at 27-days throughout the six years of high to moderate levels of solar activity. The 13-day periodicity is usually not simply a second harmonic related in phase with a 27-day fundamental. Although periodic waveforms with a 27-day periodicity that are strongly nonsinusoidal in shape would have harmonics that are related in phase with the fundamental, for solar-rotational UV variations such related harmonics are much weaker at the second harmonic than the observed 13-day periodicity. The 13-day variations of the solar UV flux are caused mostly by two peaks in solar activity per solar rotation or per 360^{o} of solar longitude. In the first halves of both 1979 and 1980, a major episode of 13-day periodicity occurred with negligible 27-day periodicity, and vice versa during their second halves. During 1981 - 1984, the episodes of 13-day periodicity were not as strongly separate from those of 27-day periodicity, but still the 13-day periodicity was usually not a second harmonic related in phase to the 27-day solar-rotational variations.

The ratios of power in the 13-day periodicity to that in the 27-day periodicity is fairly constant for photospheric UV fluxes throughout the 170 - 260 nm wavelength range, the main exception being the chromospheric Si II lines in the 180 - 182 nm range. The 13 to 27-day power ratio for the Mg II h & k line center is distinctly lower than for the 170 - 260 nm range, which is consistent with this UV flux including more chromospheric emission than in

the case of most other UV fluxes. The Mg II center-to-wing ratio agrees closely with the results for the line center, which means that Heath's UV index is a good measure of chromospheric 13-day periodicity, like that in chromospheric EUV lines, but is appreciably lower in 13-day power than the photospheric UV flux in the 170 - 260 nm range. Conversely, the Al I edge ratio has much higher power in the periodicity near 13 days relative to that near 27 days than does the solar UV flux in the 170 - 260 nm range. The 205 nm flux (also the 200 - 205 nm band) represent well the short-term variations throughout the 170 - 260 nm range. The Mg I line near 285 nm has 13-day periodicity similar to that in the 170 - 260 nm range but has a lower signal-to-noise ratio than the solar UV flux at 205 nm or in the 200 - 205 nm band.

1. NIMBUS-7 SOLAR UV SPECTRAL IRRADIANCE DATA

1.1 Six Years of Observations

The solar UV measurements studied here are from a six-year set of data tapes obtained from the National Space Science Data Center at NASA Goddard Space Flight Center, Greenbelt, Maryland 20771. This data set covers the interval November 7, 1978 through September 29, 1984, which includes the peak and main decay of solar cycle 21. These measurements of solar UV spectral irradiance from the NIMBUS-7 satellite were taken in the 160 - 400 nm wavelength range with a 1.1 nm bandpass and with 0.2 nm steps in wavelength on about three out of four days by the Solar Backscatter UV (SBUV) instrument. Dr. Donald F. Heath, Principle Investigator for SBUV, has described this instrument elsewhere (Heath and Schlesinger, 1986; Heath et al., 1975). This data set includes some corrections for long-term drifts in the instrument compared to our prior studies (Donnelly et al., 1986a,b) but does not include any revisions based on the long-term variations of the Mg II center-to-wing ratio. Supplementary data included in our analyses include the following: (1) sunspot number R from Solar Geophysical Data (SGD), (2) the Ottawa daily values of the solar 10.7 cm flux F10 from SGD, and (3) the equivalent width of the He I absorption line at 1083 nm from the National Solar Observatory (Harvey, 1984).

All solar UV instruments flown on satellites drift in instrument sensitivity with time. The NIMBUS-7 SBUV measurements show no evidence of any sudden changes in instrument sensitivity but they do show evidence of slow smooth long-term drifts. The short-term variations studied here are not affected significantly by the slow drifts in instrument sensitivity. Long-term trends, both those from solar variations and from instrumentation drifts, were removed at each wavelength studied by least-squared error fitting a twelfth order polynomial to two year intervals of data and then removing the polynomial value for each daily measurement to obtain residuals dominated by short-term variations with negligible variations over half a year or longer.

1.2 Solar UV Spectra

Figure 1.1 shows the NIMBUS-7 measurements of the solar UV spectral irradiance on its first day of measurements (Heath, 1980). Later in this report, flux units of Watts cm^{-3} are used, where 1000 W cm^{-3} = 1 W m^{-2} nm^{-1}. The main features in Figure 1.1 are the following: (a) the general fall off of flux with decreasing wavelength, (b) the Ca II H and K absorption lines near

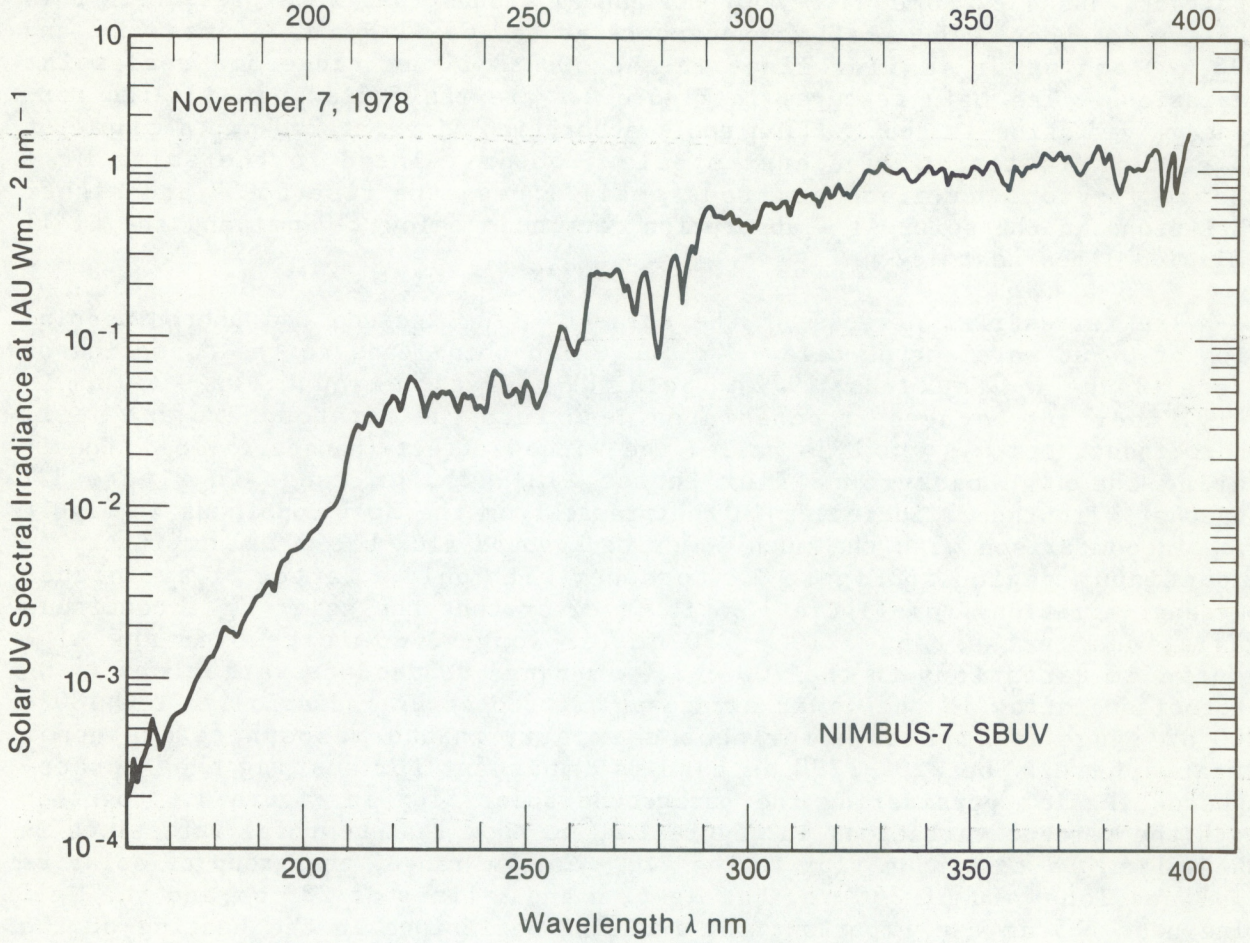

Figure 1.1 Solar UV spectral irradiance.

393 and 397 nm, seen here with low wavelength resolution relative to the wavelength structure of the core of the line, (c) the Mg I absorption line near 285 nm, (d) the Mg II h & k lines near 280 nm, which are not resolved in these measurements and appear as one large absorption line, (e) the sharp drop in solar UV flux from 260 to 250 nm related to some Fe absorption lines and the onset of Mg I continuum absorption, and (f) the rapid drop in flux from 212 to 207 nm from the onset of Al I continuum absorption in the solar photosphere, temperature minimum region and lower chromosphere. The solar spectrum changes with decreasing wavelength from predominantly absorption features to some strong emission lines starting at about 182 nm.

Figure 1.2 shows the variation of the solar UV spectral irradiance derived from Heath, Repoff and Donnelly (1984) from a study of solar rotational variations from an earlier two-year set of NIMBUS-7 SBUV measurements that did not include corrections for long-term drift, which are included in the six-year data set analyzed here in Chapters 2 - 6. The flux at a solar-rotation induced local maximum was divided by the average of the flux at the preceeding and following minima for the eight large 27-day variations discussed in Chapter 2 of Heath, Repoff and Donnelly (1984). The average offset in the 300 - 400 nm range in Figure 1.2 of about 0.2% above 1.0 is believed to be an

artifact caused by some half-year and annual trends that were present in this earlier data set. The small enhancements at the Ca II H and K lines (397 and 393 nm) and other smaller lines in the 300 - 400 nm range are real solar variations. The main features in Figure 1.2 are the following: a large percentage variation in the Mg II h and k absorption lines at 280 nm, a couple of percent variation at wavelengths below 250 nm related to the solar Mg I absorption continuum and numerous small lines, the rise to 5% and higher variations in the solar Al I absorption continuum below 210 nm, and the Si II emission lines near 182 nm.

The terrestrial effects of the solar UV flux include the photodissociation of O_2 at wavelengths below 242 nm, which then leads to the formation of ozone (Banks and Kockarts, 1973). Solar UV radiation around 200 - 230 nm is very important because it penetrates deep into the stratosphere and still photodissociates O_2, which is called the window effect (Hanson, 1978). Considering the high background flux in the 210 - 253 nm range in Figure 1.1 together with the 2% increases in that range from the Mg I continuum in Figure 1.2, in comparison with the much lower background flux below 210 nm in the Al I continuum region in Figure 1.1 together with only a factor of two higher percent variation from Figure 1.2, it is clear that the solar Mg I continuum variations in the range 210 - 230 nm (or longer) dominate over the Al I continuum variations in the 200 - 210 nm range to produce variations in O_2 photodissociation in the lower stratosphere. Solar UV radiation in the 180 - 200 nm range is important for photochemistry in the mesosphere and upper stratosphere. The 220 - 290 nm band is important for heating the stratosphere. Again, considering the background solar flux in Figure 1.1 together with the percent variations in Figure 1.2, we know that temporal variations in the solar Mg I continuum flux in the 220 - 253 nm range, the group of solar Fe II lines longward of 260 nm, the Mg II h and k lines at 280 nm and the Mg I line near 285 nm are important for inducing variations in the heating of the stratosphere. Considering the low accuracy in the percent variation near 270 nm and in the far wings of the Mg II and I lines together with the high background flux at these wavelengths, the importance to stratospheric heating from solar variations at these wavelengths is not yet clearly determined.

1.3 Heath's Mg II UV Index

Heath and Schlesinger (1986) defined the center-to-wing ratio for the Mg II h and k solar absorption lines (not resolved into two lines because the spectrometer bandwidth is too broad) by the following equation:

$$R(MgII,t) = \frac{4[F(279.8\ nm,\ t) + F(280.0\ nm,\ t) + F(280.2\ nm,\ t)]}{3[F(276.6,t) + F(276.8,t) + F(283.2,t) + F(283.4,t)]} \quad (1)$$

where F(w,t) is the measured solar flux at wavelength w and time t. We consider this ratio to be extremely important to measurements of solar UV flux variations. Therefore, we have included it in our analyses in this report and would like to introduce the reader to its features. R(MgII) is sometimes referred to below as UV1 or Heath's UV index.

The numerator gives the flux at the center of the line, where the flux is lower than in the wings of the line, as shown in Figure 1.1, but the percent

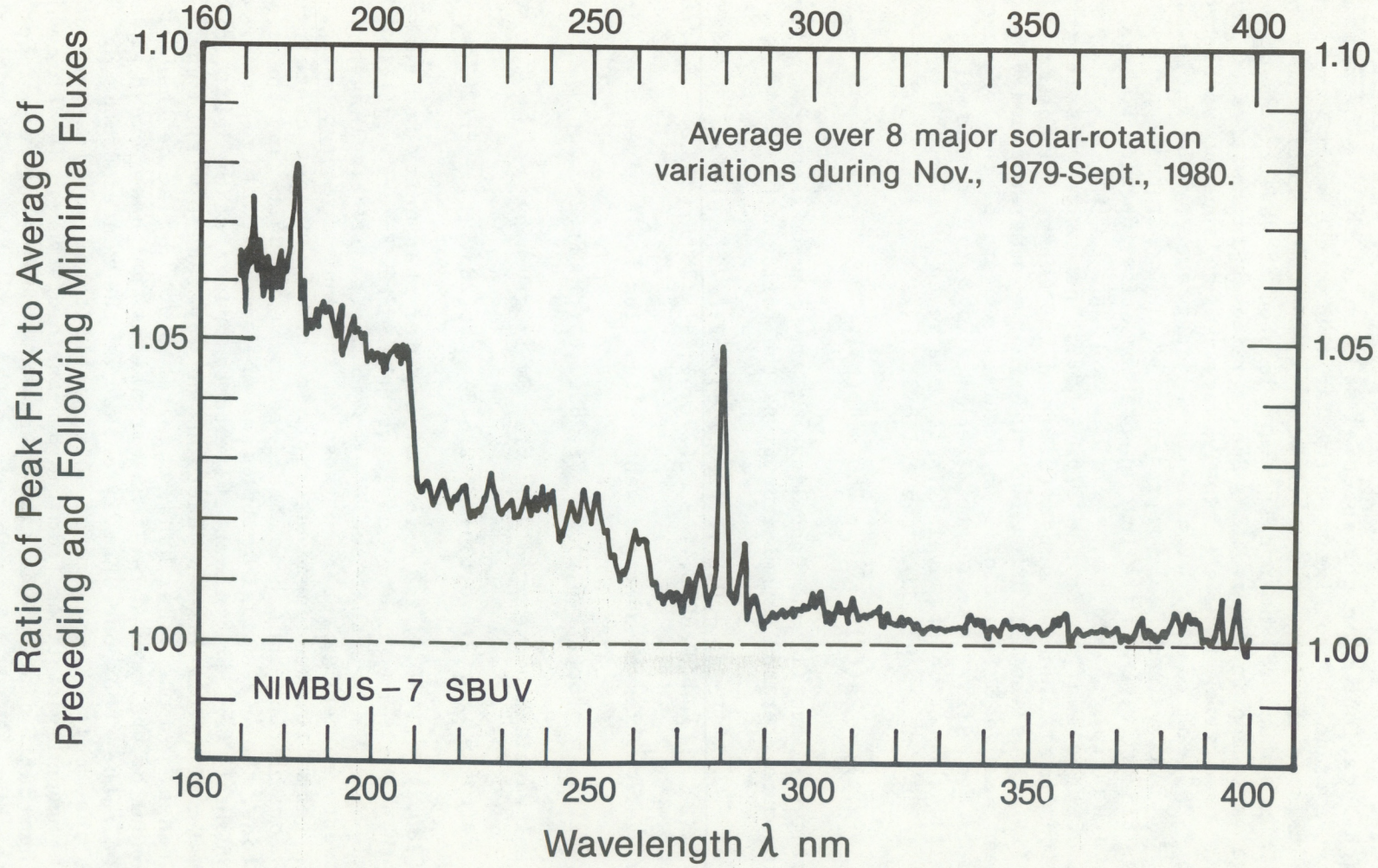

Figure 1.2 Fractional solar-rotational variation as a function of wavelength.

variation with solar activity is very high. The average of three flux values is used because this average is much less sensitive to the effects of any small jitter in the wavelength drive system, i. e. small fluctuations in wavelength locations from one spectral scan to another. The denominator includes an average of two fluxes in the far wing of the short wavelength side and two fluxes in the long-wavelength wing, where their spacing in wavelength is symmetrical about 280 nm and they are located at wavelengths of very low percentage variation in Figure 1.2. Such a ratio is insensitive to drifts in instrument sensitivity that are slowly varying functions of wavelength over the 276.6 - 283.4 nm range, which can be demonstrated by the following: Let the measured flux values Fm be represented by the separated functions of the real solar flux Fr(w,t) and the instrumentation drift function D(w,t), where w represents wavelength and Fm = FrD. As long as D is a weakly varying function of wavelength over the 276.6 - 283.4 nm range (possibly a large change with time), then the substitution of FrD values for the Fm values in equation (1) allows the factoring out of D in the numerator and denominator, which means Heath's MgII ratio is an accurate measure of the true center-to-wing ratio. Even if the wavelength dependence of D is not so small, if it is nearly a linear function of wavelength for the seven wavelengths involved over the 276.6 - 283.4 nm range, like the following:

$$D(w,t) = a(t)[1 + (w - 280\ \text{nm})b(t)]. \qquad (2)$$

Substituting (2) into (1) and canceling out the common factor a(t) from each term in the numerator and denominator gives the following:

$$R(MgII) = \frac{Fc(t) + 0.2b[Fr(280.2,t) - Fr(279.8,t)]/3}{Fw(t) + \{3.4b[Fr(283.4) - Fr(276.6)] + 3.2b[Fr(283.2) - Fr(276.8)]\}/4} \qquad (3)$$

where the real wavelength-averaged center-line flux Fc is given by

$$Fc(t) = [Fr(279.8,t) + Fr(280.0,t) + Fr(280.2,t)]/3, \qquad (4)$$

and the real wavelength-averaged wing flux Fw is given by

$$Fw(t) = [Fr(276.6,t) + Fr(276.8) + Fr(283.2,t) + Fr(283.4,t) \qquad (5)$$

Since $Fr(280.2) \cong F(280.4)$ and b is much smaller than unity for these wavelengths, then the terms in the numerator other than Fc are negligible. From Figure 1.1, one can see that the fluxes in the short-wavelength wing are roughly twenty percent lower than those in the long-wavelength wing, so the remaining terms in the denominator other than Fw do not cancel to zero. However, considering that b is small relative to unity and there are two subtractions, these residual drift terms are small relative to Fw. Consequently, R(MgII) is fairly insensitive to instrumentation drift, including drifts that are nearly linear functions of wavelength within the 276.6 - 283.4 nm range. On the other hand, this ratio would also be insensitive to any component of the real solar flux variations that has a broad wavelength dependence rather than one sharply peaked at the center of the Mg II line. Note also that this UV measure of solar activity is unitless and does not include the annual variations from the Sun-Earth distance. The flux variation from the Sun-Earth distance is like a common multiplying factor for each F term in equation (1) and those factors in the numerator cancel with the ones in the denominator.

1.4 Al I Edge Ratio

A second feature in the solar spectrum where there is a rapid change in solar variability over a short change in wavelength is at the Al I absorption edge near 208 nm in Figure 1.2. Heath and Schlesinger (1986) defined their Al I edge ratio as follows:

$$R(AlI,t) = B(t)\frac{F(208.6,t) + F(208.8,t) + F(209.0,t)}{F(211.2,t) + F(211.4,t) + F(211.6,t)} \quad (6)$$

which is primarily a ratio of an average of flux at three wavelenths at the short wavelength side of the edge to a similar average from the long-wavelength side. The corresponding terms in the numerator and denominator are 2.6 nm apart in wavelength. The B term attempts to correct for the wavelength dependence of the instrumentation drift function over this 2.6 nm interval by taking the average of two similar ratios with wavelength separations of 2.6 nm as follows:

$$B(t) = 2/\{\frac{[F(203.4,t) + F(203.6,t) + F(203.8,t)]}{[F(206.0,t) + F(206.2,t) + F(206.4,t)]} + \frac{[F(213.8,t) + F(214.0,t) + F(214.2,t)]}{[F(216.4,t) + F(216.6,t) + F(216.8,t)]}\} \quad (7)$$

where the percent variation due to solar activity is essentially the same in the numerator as that in the denominator for each fraction in B. See Figure 1.2.

Because the effects of a small jitter in the wavelength drive is important when studying the temporal variations of a deep and narrow absorption line, we use the average of flux data from two or three adjacent wavelength steps nearest the center of the line, three in the case of the unresolved Mg II h & k lines. From the viewpoint of small random measurement noise other than that due to wavelength jitter, the noise affecting the numerator in (1) is the same as that involved in looking at the line flux alone rather than using the ratio. The noise from the denominator would be of the same order as that of the numerator, which suggests that the small random noise or isolated noise spikes in R(MgII) would be comparable or a slightly greater problem than that in the flux measurements at the center of the Mg II h & k lines. Considering the large solar variability signal in the center of the line, as shown in Figure 1.2, we expect an excellent signal to noise ratio in R(MgII). While R(MgII) involves seven flux measurements, R(AlI) involves eighteen. While the solar signal in the center of the Mg II line is six times or more stronger than that in the wings (Figure 1.2), the solar signal in the Al I edge at 208.8 nm is less than twice that at 211.4 nm. Consequently, we expect the ratio of solar signal to random observational noise to be much poorer in R(AlI) than in R(MgII) and we expect a more frequent occurrence of noise spikes with respect to time in the Al I edge ratio than in the Mg II center-to-wing ratio.

1.5 Si II Lines with Background Removed

Si II emission lines appear in Figure 1.2 as a spike just below 182 nm. To determine whether the temporal characteristics of these lines were

different than those of the Al I continuum at adjacent wavelengths, we computed the following:

$$F(SiII,t) = [F(181.6,t) + F(181.8,t) - F(177.8,t) - F(183.0,t)]/2 \quad (8)$$

The first two terms to the right of the equal sign in equation (8) give a two wavelength-step average of the local peak caused by two unresolved Si II lines while the last two terms estimate the Al I background flux. Equation (8) is like that used in case A, table 3.2, of Puga et al. (1987), except here we used just two wavelengths for the line center rather than three. Equation (8) is useful only for studies of short-term variations. Because of the small difference calculation involved, we expect the result to be noisier, or have a lower ratio of solar signal to observational noise, than any of the individual fluxes involved.

2. TIME SERIES OF SHORT-TERM RESIDUALS

The NIMBUS-7 data were analyzed for the following three types of data sets: (1) averages over 5 nm bands (160 - 165, 165 - 170, etc.), (2) the flux at individual wavelength settings selected for certain features in Figure 1.2, and (3) the special ratios and revised fluxes R(MgII), R(AlI) and F(SiII). These data sets were divided into two year intervals (January 1, 1979 - December 31, 1980; 1980 - 1981; 1981 - 1982; 1982 - 1983 and 1983 - Oct. 29, 1984) as well as the original six year data set from November 7, 1978 - October 29, 1984. Each of these data sets were then least-squared-error fit with a twelfth order polynomial, which was used to estimate the long-term (years) and intermediate-term (several months) variations in the data. The polynomial value was then subtracted from the original data leaving residuals containing the short-term variations. These residuals were then used in all of the analyses discussed in the rest of this report. The analysis techniques used here are the same as those discussed in Chapters 4 - 7 of Heath et al. (1984) and by Lean and Repoff (1987).

Figures 2.1 - 2.6 show yearly graphs of a small sample of these time series. The top graph looks very similar in the relative shape of the temporal variations to those of the middle graph in each of these figures. Indeed, most of the time series studied have very similar temporal shapes to those of the top two graphs in each of these figures. The bottom graph tends to have more fine structure than the top two graphs, partly because it is noisier, which was discussed in section 1.4, and partly because it is very strong in 13-day periodicity, which will be discussed further in Chapters 5 and 6.

Note in Figure 2.1 that peaks occur about every 13 to 14 days from mid January through May, which has been extensively discussed elsewhere (Donnelly et al., 1982, 1983, 1984, 1985, 1986a,b; Donnelly, 1983; Heath et al. 1984). The main peaks in Figure 2.1 are about 28 days apart in June - December. In Figure 2.2, there is again strong 13-day periodicity from late January through April and 28-day peaks from May through November, 1980. In Figure 2.3, there is more of a mixture of 28 and 13-day peaks rather than separate episodes of either predominantly 13-day peaks or other episodes of primarily 28-day peaks. In 1982, there is an excellent example of an episode of major activity developing in June and causing very large solar rotational variations in July, August, Sept., and Oct., with a rejuvination of the activity at slightly different solar longitudes in Nov., which causes a slight phase delay in the 28-day variations, with peaks in Nov., Dec., 1982, and Jan., Feb. and March, 1983. In Figure 2.6, 13-day periodicity is again evident. Note that the Al I edge ratio appears to be richer in fine structure relative to the 28-day and 13-day variations in the 200 - 205 and 175 - 180 nm bands during October 1983 to October 29, 1984 than for the earlier years of data.

Summarizing, 13-day periodicity is strong throughout the six year period and is more mixed in with the 28-day periodicity in 1981 - 1984 than in 1979 - 1980, with the exception of the strong episode of predominantly 28-day variations from June - Oct., 1982. The strongest amplitude short-term variations are the 28-day variations and the 13-day variations are the second strongest. The temporal variations appear to have similar shapes (but different amplitudes of course) at the various UV wavelengths, except the temporal variations of the Al I edge ratio appear to be richer in fine structure.

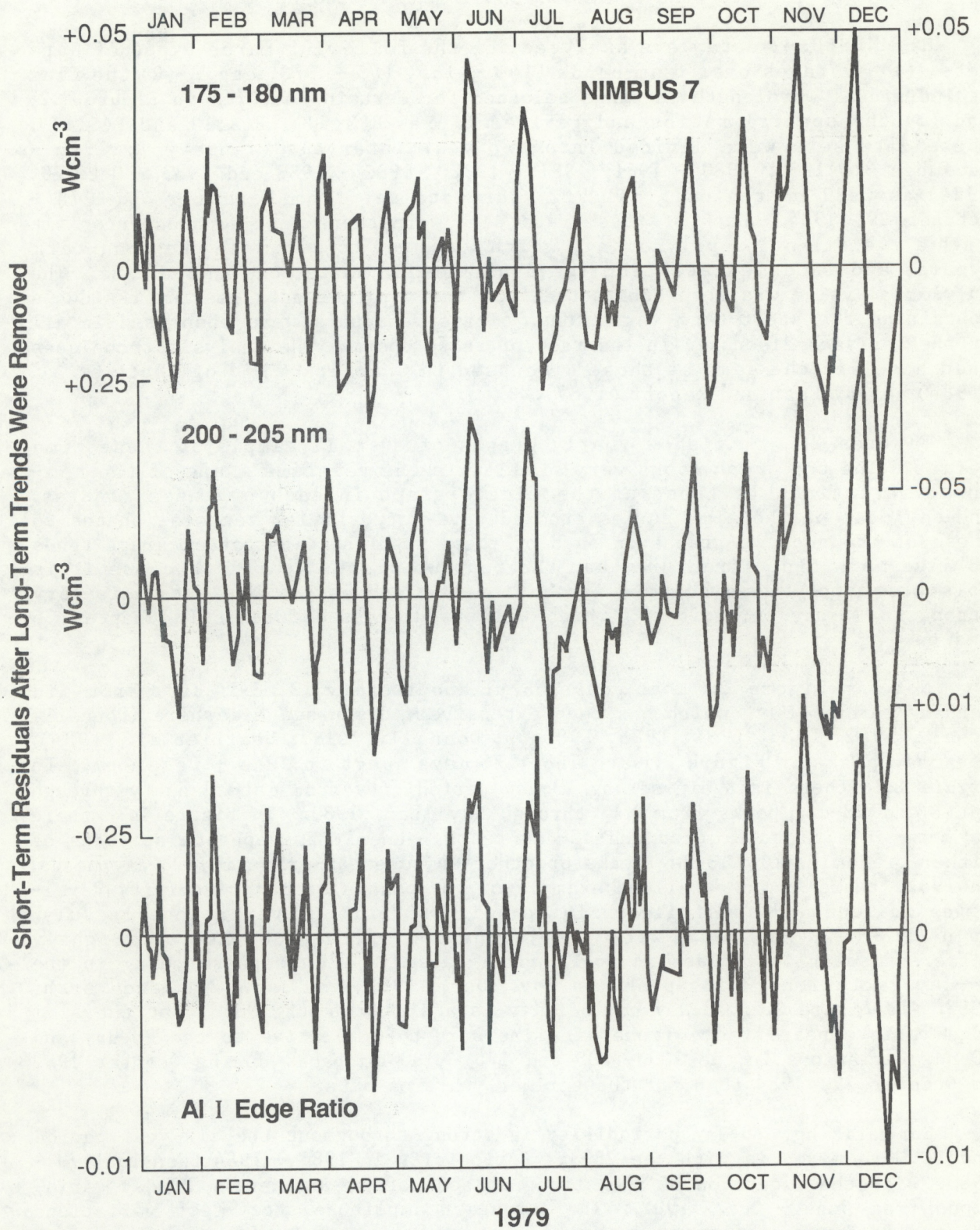

Figure 2.1 Time dependence of example short-term residuals for 1979. Similar residuals for the UV flux at 205 nm measured by the NIMBUS-7 satellite and the equivalent width of the He I absorption line at 10830 A from mountain-top measurements of the National Solar Observatory for Nov. 7, 1978 - Nov. 6, 1982, were published by Donnelly et al. (1983).

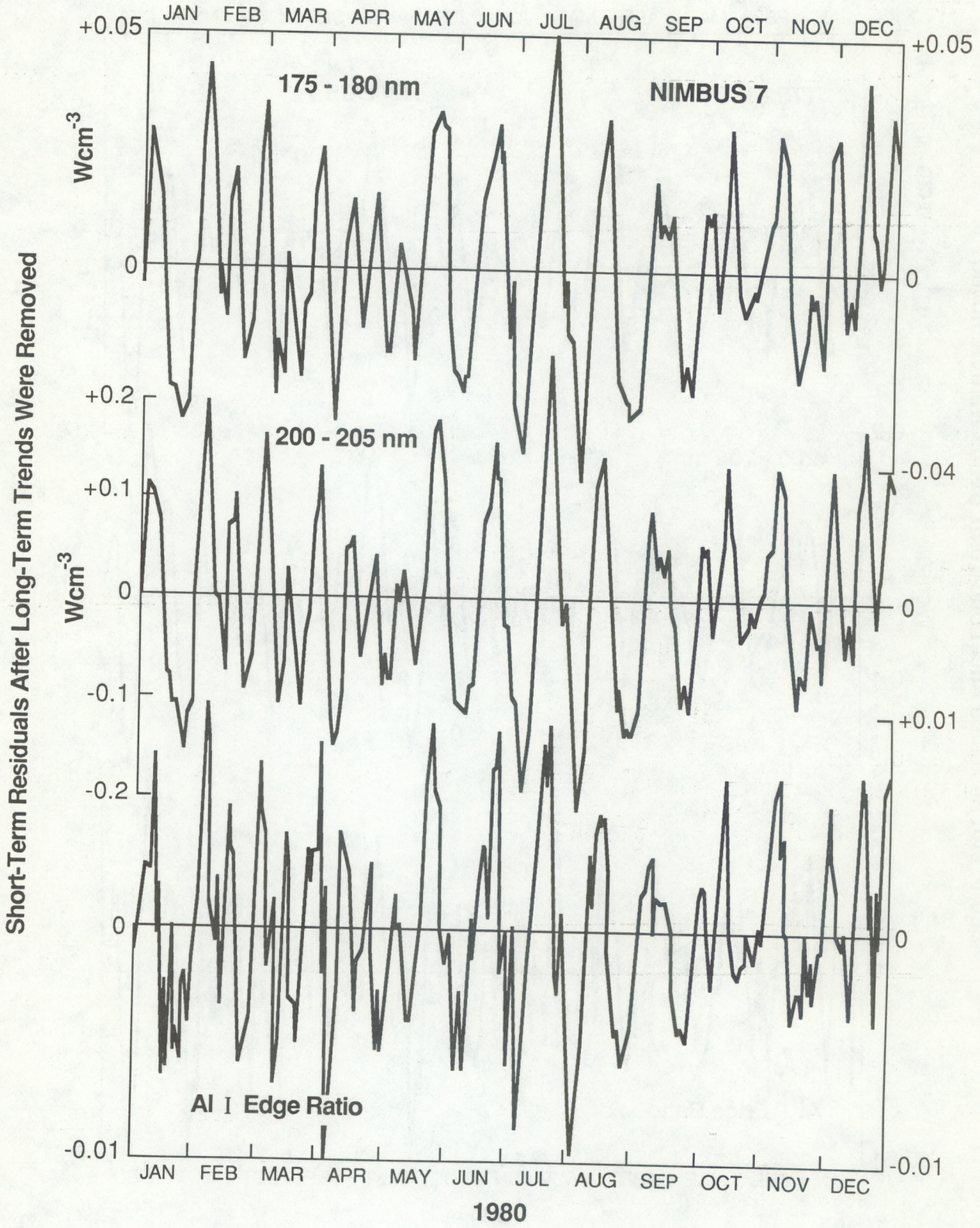

Figure 2.2 Time dependence of example short-term residuals for 1980.

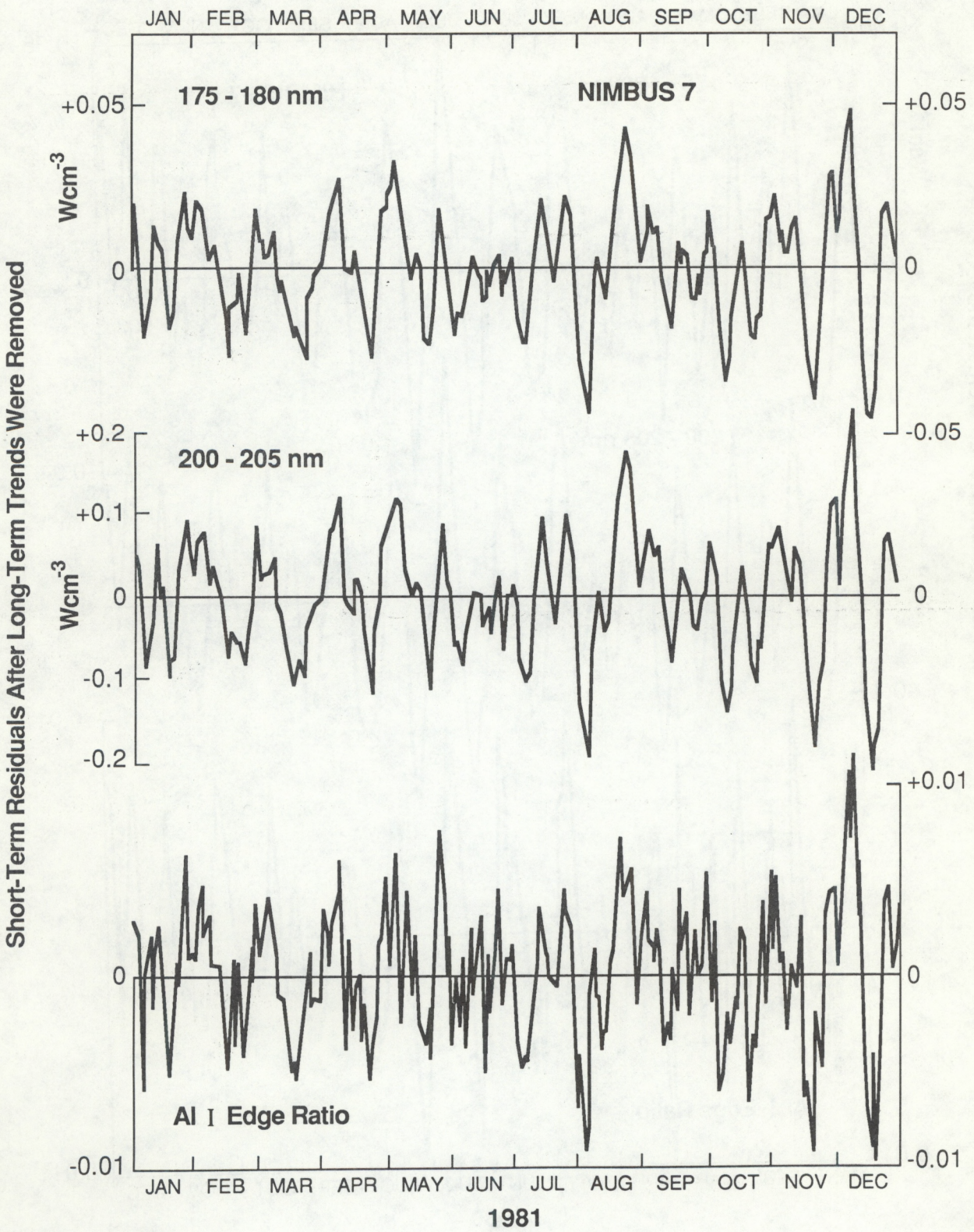

Figure 2.3 Time dependence of example short-term residuals for 1981.

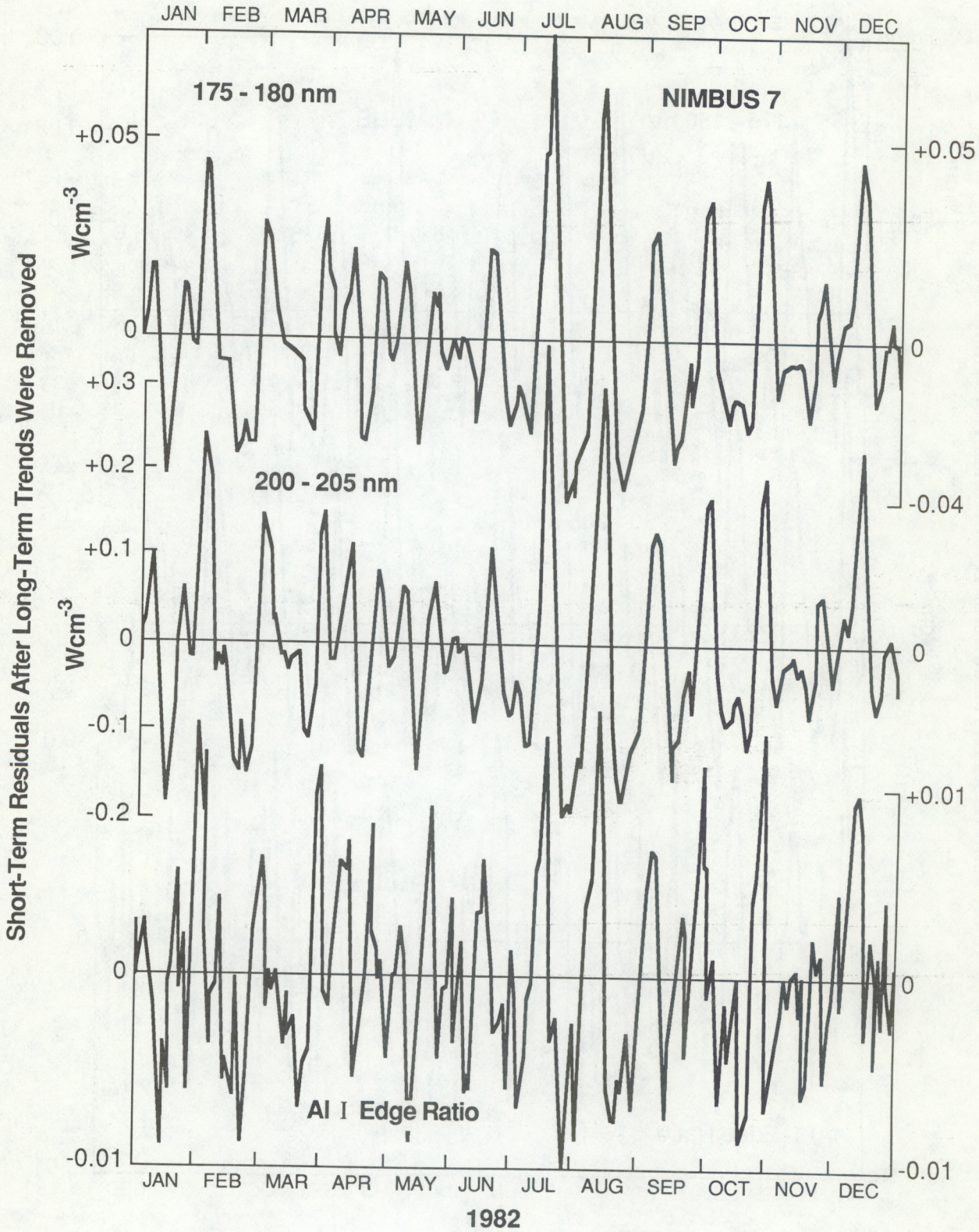

Figure 2.4 Time dependence of example short-term residuals for 1982.

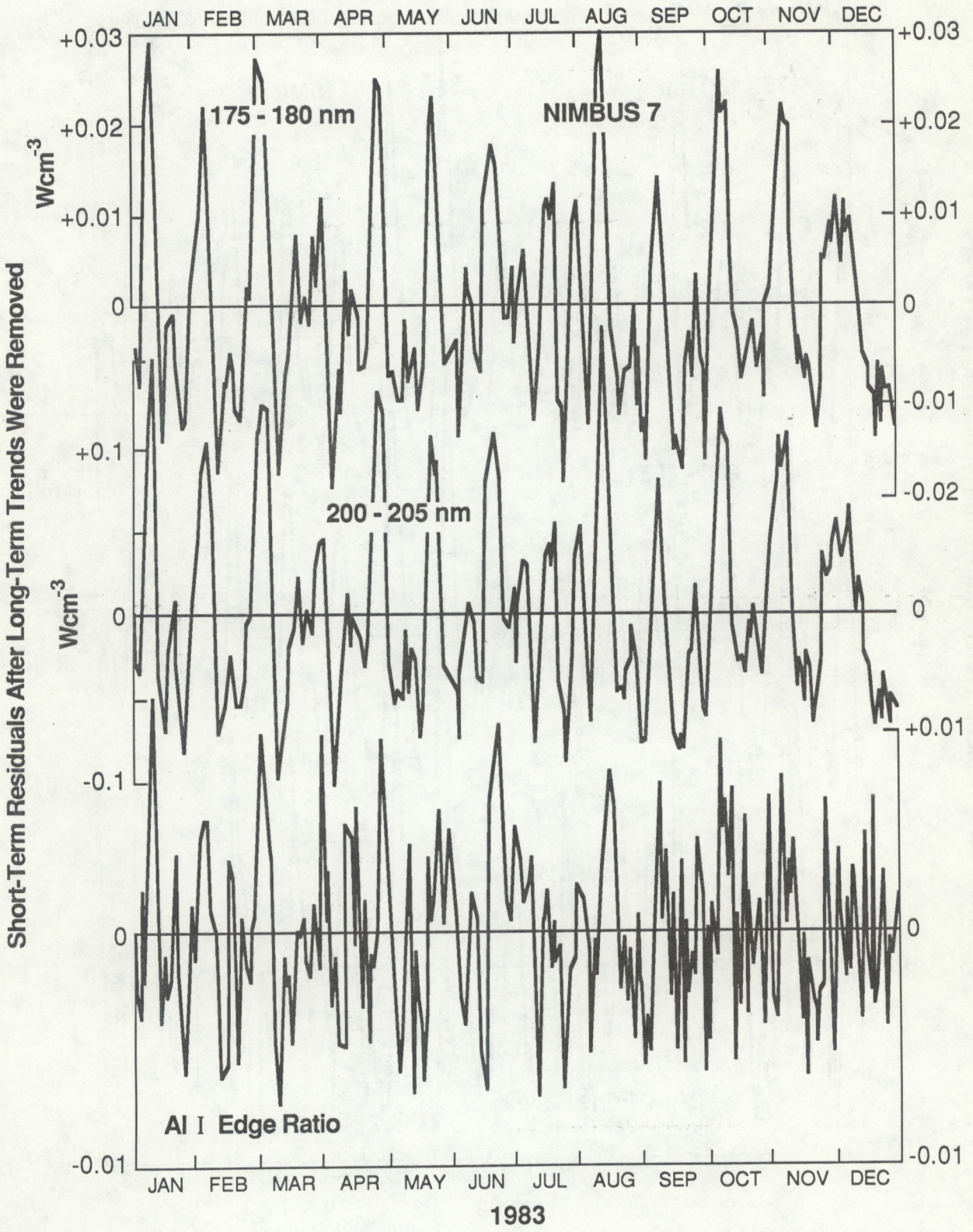

Figure 2.5 Time dependence of example short-term residuals for 1983.

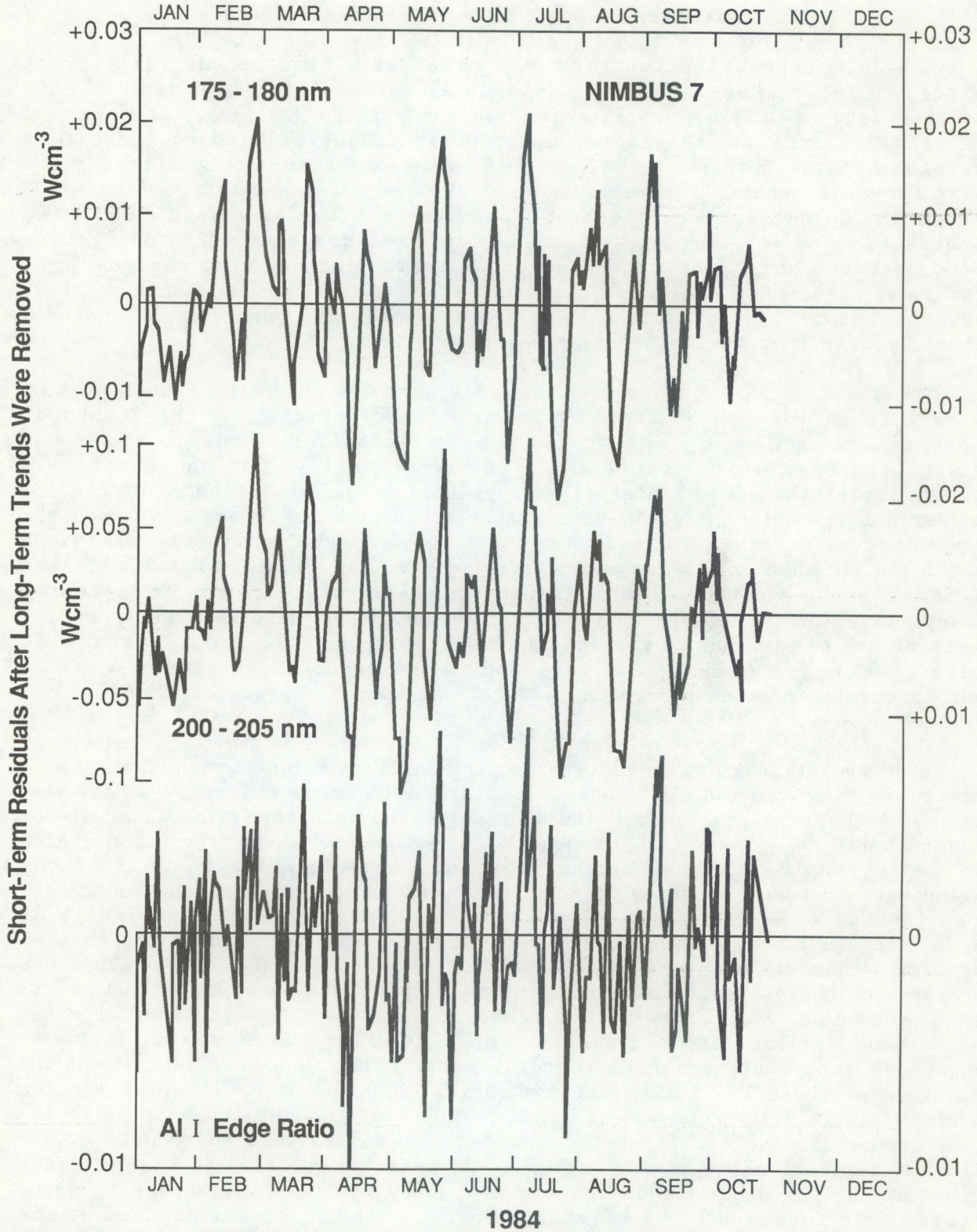

Figure 2.6 Time dependence of example short-term residuals for 1984. The latest data available for this study were measured on September 29, 1984.

3. AUTOCORRELATION ANALYSES

3.1 Uniformity of Short-Term UV Flux Variations

The autocorrelation function (AF) compares a time series with itself shifted to later times. Figure 3.1 shows AF values for 1979 - 1980 UV data for time lags of integer numbers of days from zero to 365 days. At zero lag, the original data and the lagged data set are identical and the result is therefore unity. For one or two days of lag, AF decreases only slightly for solar UV data, because active region evolution and solar-rotation induced UV variations do not produce strong temporal variations over such short time intervals. However, for lags of 4 to 10 days, AF drops rapidly to negative values because solar-rotation induced variations cause great changes in UV fluxes over that time scale. At lags near 28 days and integer multiples of 28 days, AF returns to peak values because the flux during one rotation compares favorably with that during adjacent solar rotations.

The shape of AF in the valleys near 14 days and odd-integer multiples of 14 days is influenced by the 13-day periodicity evident in the graphs of Chapter 2. In the case of Figure 3.1, the valleys for the curves on the top half of the figure have fairly flat and broad valleys for the first five valleys rather than deeper sharper valleys because of the influence of the 13-day periodicity evident in the time graphs of Chapter 2. When we shorten the time interval involved to less than one year and center this time window on one of the episodes of 13-day periodicity apparent in Figure 2.1 and 2.2, then AF forms peaks near integer multiples of 13 days, i. e. the former flat valleys rise into additional new peaks. Therefore, AF depends greatly on the width of the time window used and on its location in time according to what episodes of major activity are included in the window. We have chosen two year intervals in order to include several episodes of major activity.

The most important result in Figures 3.1 - 3.3 is the great uniformity in the autocorrelation functions for the various UV wavelengths involved for a particular time window. In contrast to this uniformity for solar UV fluxes, Figure 3.4 shows a great diversity of results for this same time interval for chromospheric EUV fluxes (H Lyman beta), chromosphere-corona transition region EUV radiation (Fe IX) and coronal EUV emission (Fe XVI), as well as for various ground-based measures of solar activity. The causes of the nonuniformity in Figure 3.4 have been discussed by Donnelly (1987). Similarly, AF showed close uniformity as a function of UV wavelength for each of the following time windows: 1980 - 1981, 1981- 1982, 1982 - 1983, and 1983 - 1984. We interpret this close uniformity as simply being a consequence of the UV activity sources that contribute to the temporal variations being essentially the same in spatial location and source temperature for the different UV wavelengths so that their relative temporal variations are nearly the same. The amplitude of these UV flux variations vary with wavelength, like the spectra shown in Figure 1.2. This wavelength dependence of the amplitude of UV variations occurs because the strength of particular solar lines and continua vary with wavelength for the regions of enhanced emission relative to the quiet sun emission. On the other hand, the temporal shape of these variations is quite uniform as a function of UV wavelength because the latter are caused by the evolution and passage across the solar disk of essentially the same spatial regions of enhanced emission.

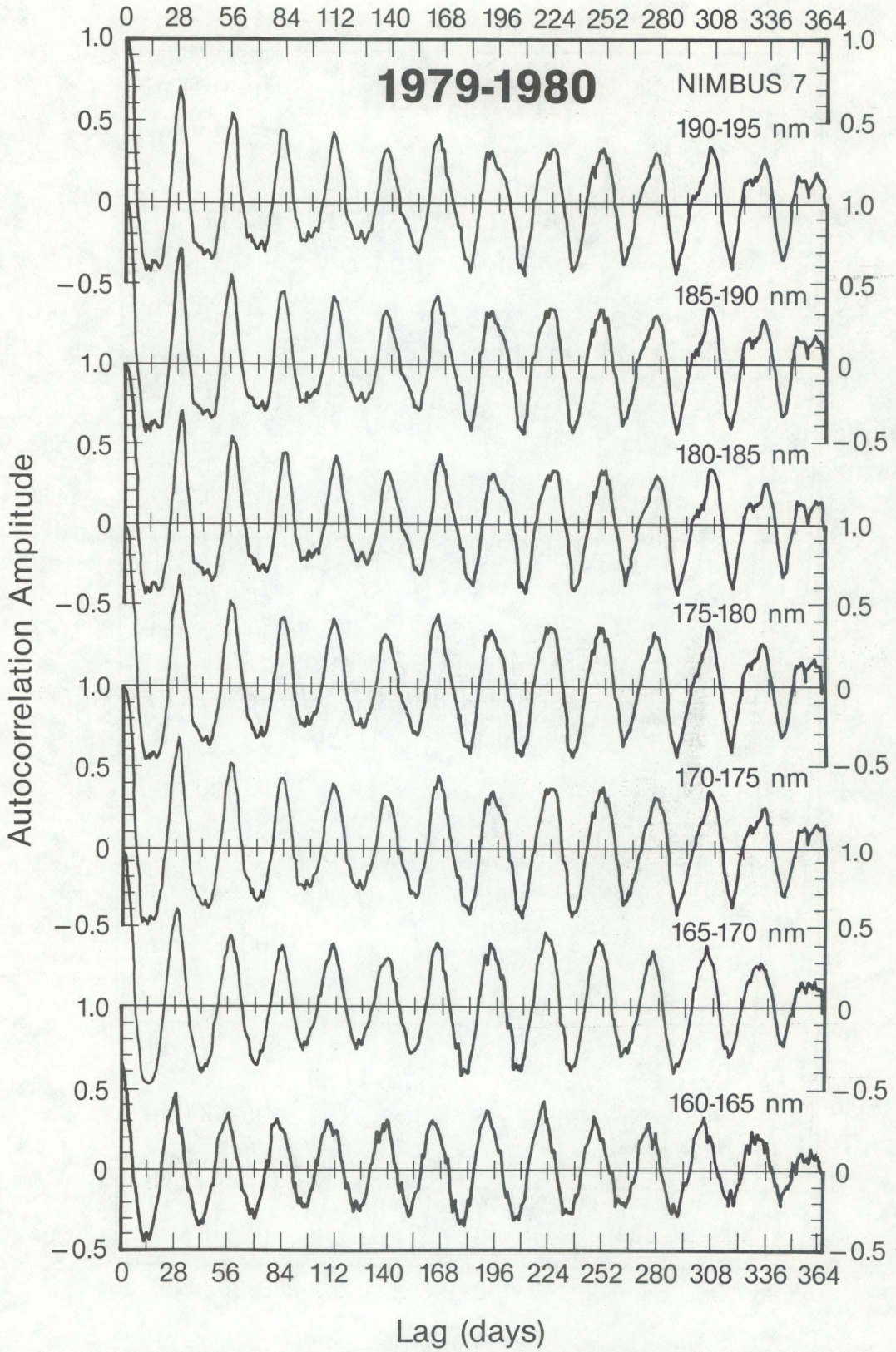

Figure 3.1 Autocorrelation functions for 5 nm bands from 160 to 195 nm. Note the strong uniformity in the autocorrelations for all wavelengths shown.

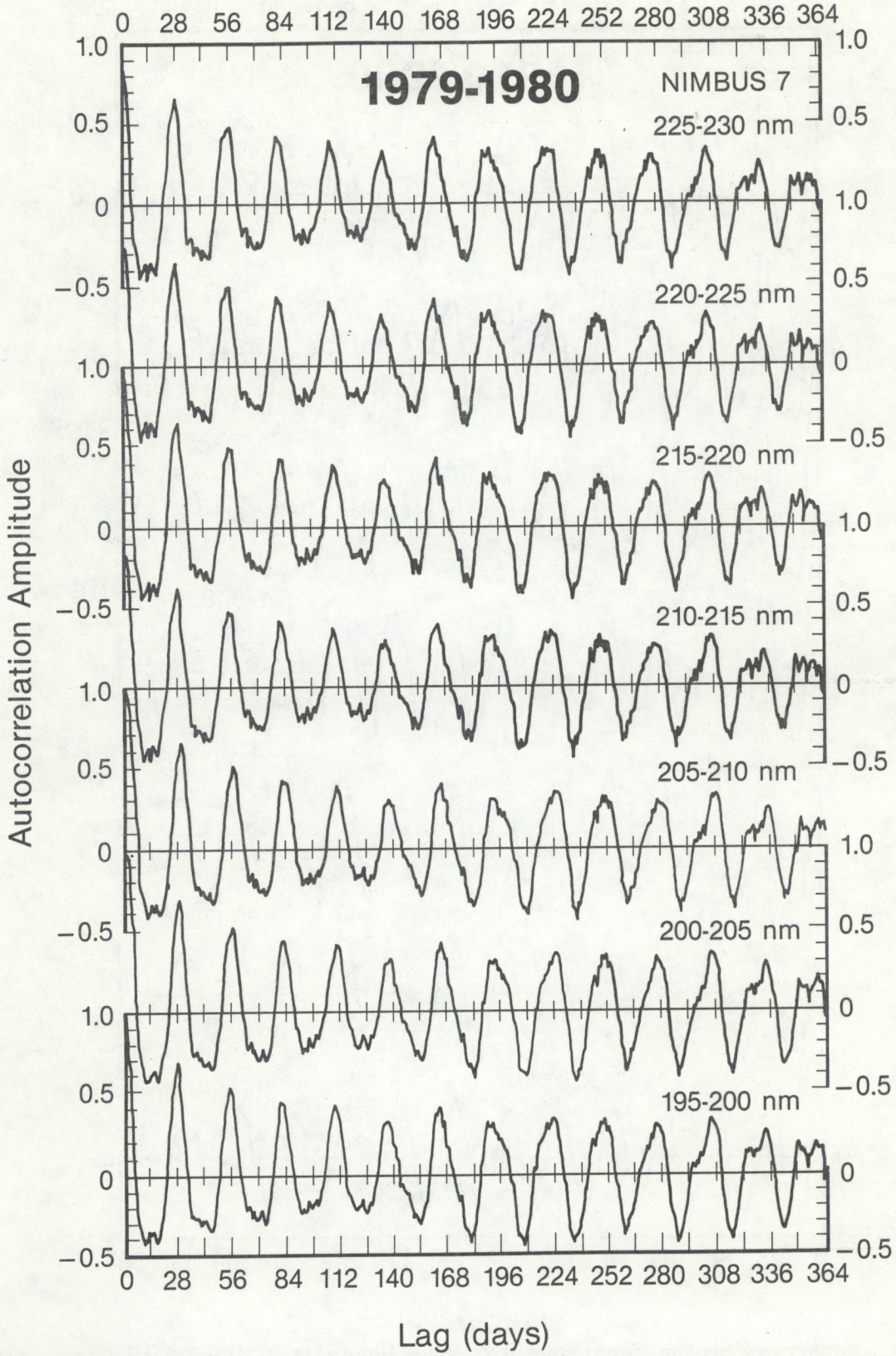

Figure 3.2 Autocorrelation functions for 5 nm bands from 195 to 230 nm. Note the slight increase in amplitude for the peak near 168 days of lag.

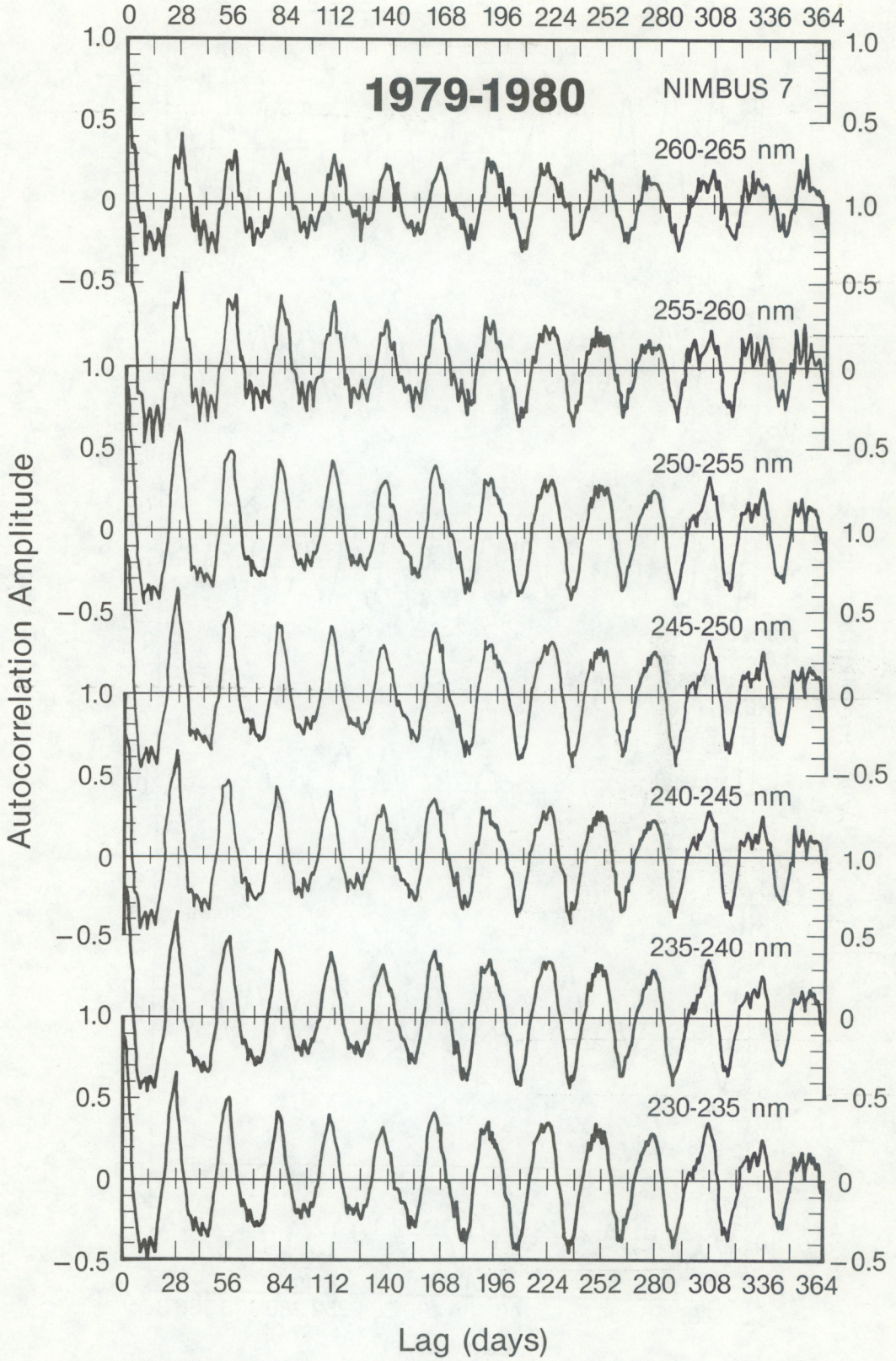

Figure 3.3 Autocorrelation functions for 5 nm bands from 230 to 265 nm. Note the small 4-day modulation, especially in the 255 to 265 nm range.

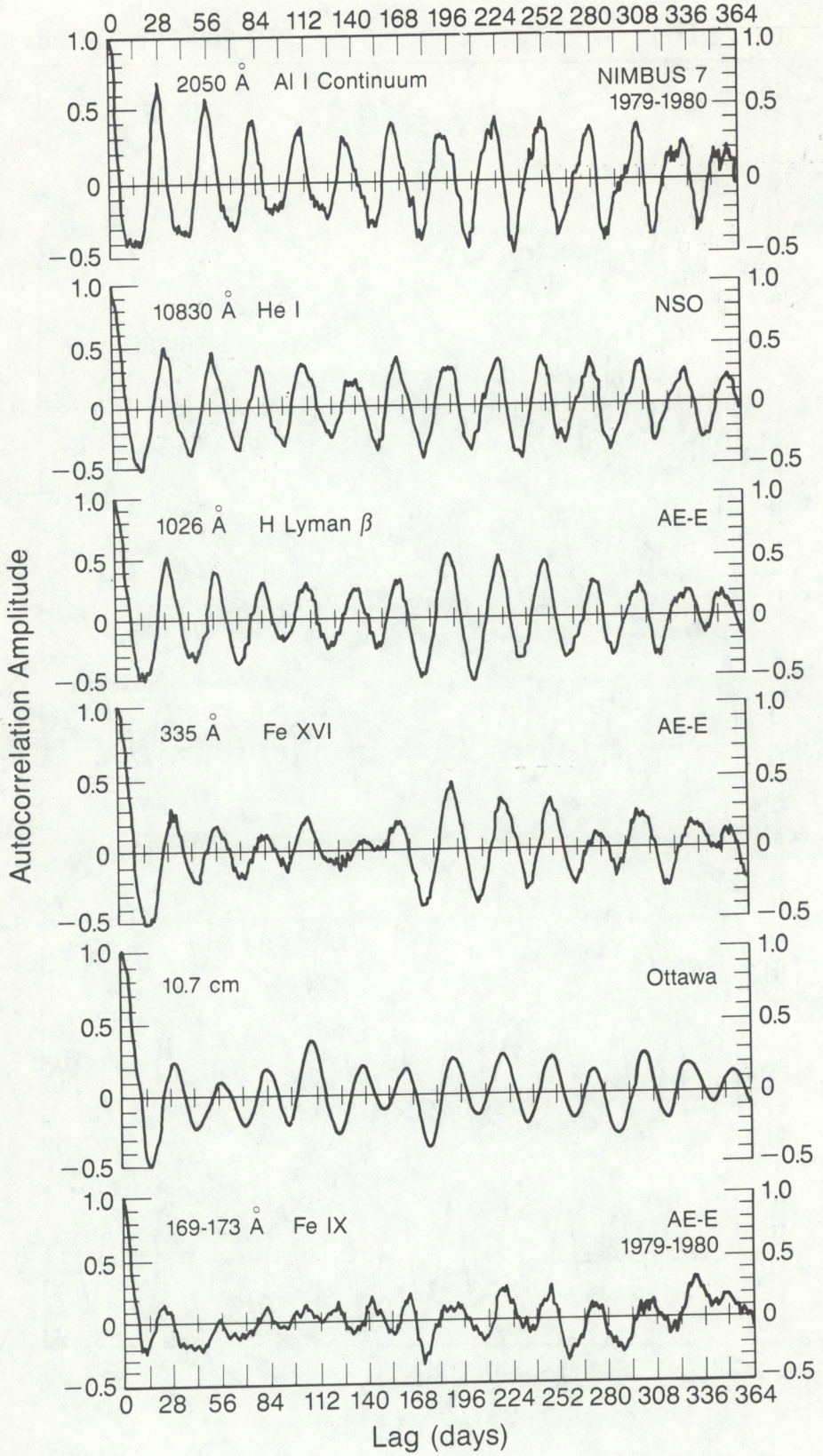

Figure 3.4 Autocorrelation functions for UV and EUV wavelengths and ground-based measures of solar activity, from Donnelly (1987).

Some small differences occur among the AF curves in Figures 3.1 - 3.3. For example, the first four valleys vary from narrow and slightly pointed to broad and flat with minor bumps from the top to the bottom of Figure 3.1. This valley trend is the same as that in the 13- to 27-day power ratios that will be discussed further in Chapter 5 and interpreted as being caused by the UV flux near 160 nm being more from chromospheric sources while that from 190 nm is mostly from the upper photosphere. Another minor difference is that the AF results for 255 - 260 and 260 - 265 nm include a stronger fine structure with a period of four days. This four-day periodicity results from an observational noise related to the four day measurement cycle (three days of observations followed by one day off). In some cases, measurements of the solar UV flux were made on these fourth days, but because the other instruments on the satellite were turned off, the spectrometers operating temperature was different on these fourth days, causing a shift in the measured UV flux. The measurements made on such fourth days were not included in this study. The remaining fourth day problem is caused by the missing data on the fourth days and by minor structure in the remaining three days per four day observing cycle. This small noise is more noticeable in the 255 - 260 and 260 - 265 nm bands because the strength of the solar signal is weaker there, as shown in Figure 1.2. For the 290 - 295 nm band and longer wavelengths (not shown in figures 3.1 - 3.3), the fourth day noise dominates AF and the solar rotation variations are weakly evident, which is consistent with the weak solar signal there in Figure 1.2.

One feature of Figure 3.4 is that the rotational peaks rise to higher values with increasing lag near either six or seven rotations of lag (near 168 or 196 days of lag). This corresponds to the partial alignment of the rotational peaks of one episode with those of another in the lagged data, i. e. the average spacing between major episodes of activity for this time interval. This same feature is only weakly evident in Figures 3.1 - 3.3, because at UV wavelengths the rotational peaks in AF decay very little during the first five solar-rotations of lag. So the increase in rotational peak amplitude from the peak near five rotations of lag to that at six rotations is small for the UV flux.

3.2 Similarity of Mg II UV and Chromospheric EUV Flux Variations

Figures 3.5 - 3.9 show the autocorrelation function for five two-year intervals for three sets of solar UV data based on NIMBUS-7 measurements and three ground-based measures of solar activity. For any one of these six data sets, the AF results vary from one two year interval to the next because what episodes of 27-day or 13-day variations are included in a two year interval varies. The UV data sets include the flux at 1 AU at 205 nm, Heath's UV index (Mg II center-to-wing ratio) and the Al I edge ratio. Comparing Figure 3.1 with the 205 nm results in Figure 3.5 shows that the UV flux at most wavelengths in the 170 - 260 nm range has temporal variations shaped very similarly to those of the 205 nm flux. Close agreement occurred for all the time intervals studied, which shows that the short-term temporal variations (days, weeks, a few months) of the 205 nm flux are similar in shape to those in the 170 - 260 nm range, only their amplitude varies with wavelength (Figure 1.2).

The autocorrelation function for the Mg II center-to-wing ratio shown in Figures 3.5 - 3.9 is essentially identical to that for the Mg II center-of-line flux (not shown), so Heath's UV index has the nice feature that, besides being insensitive to instrument drift problems and therefore a good measure of

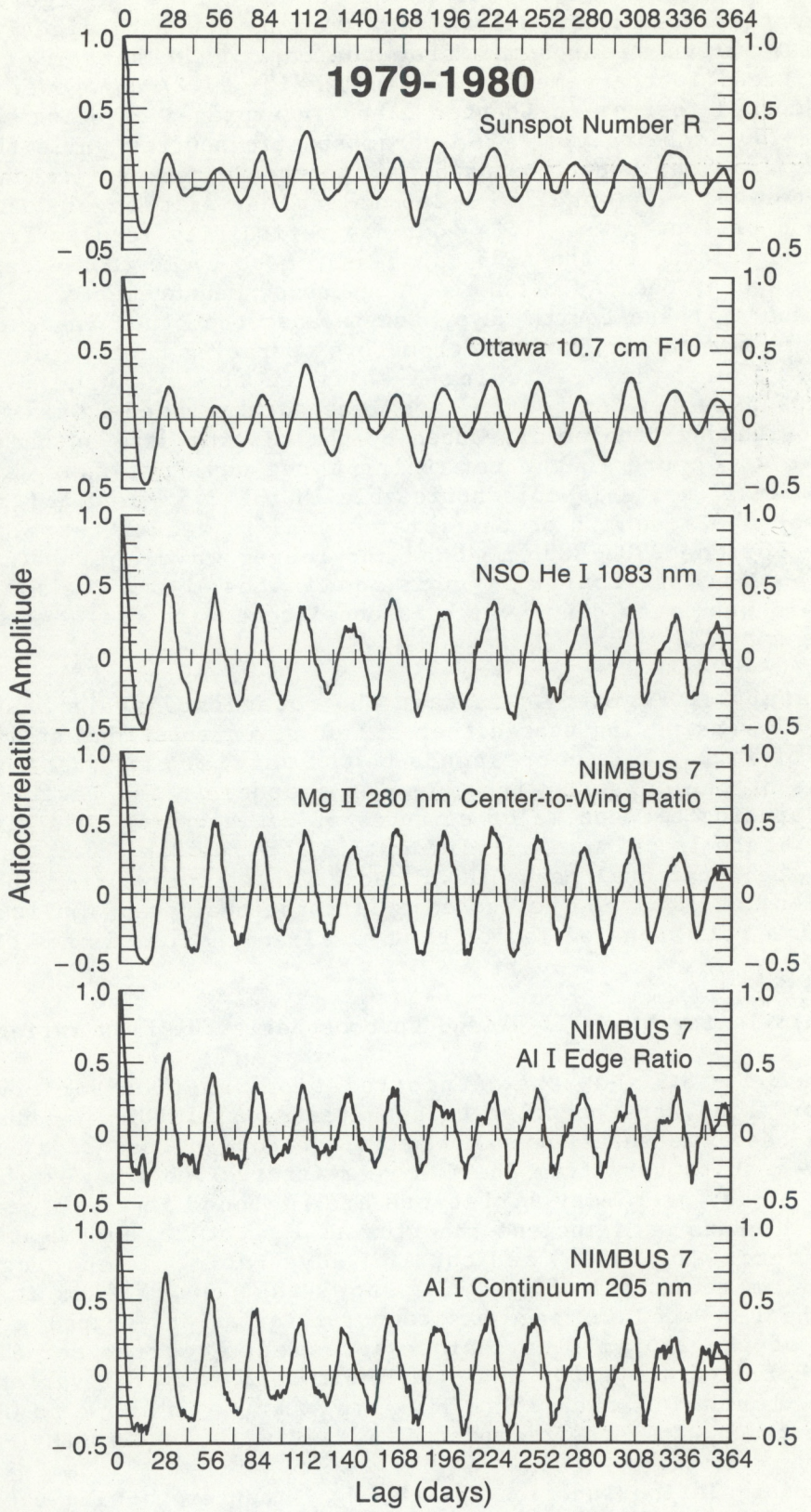

Figure 3.5 Autocorrelation functions for representative UV measurements and ground-based measures of solar activity for 1979 - 1980.

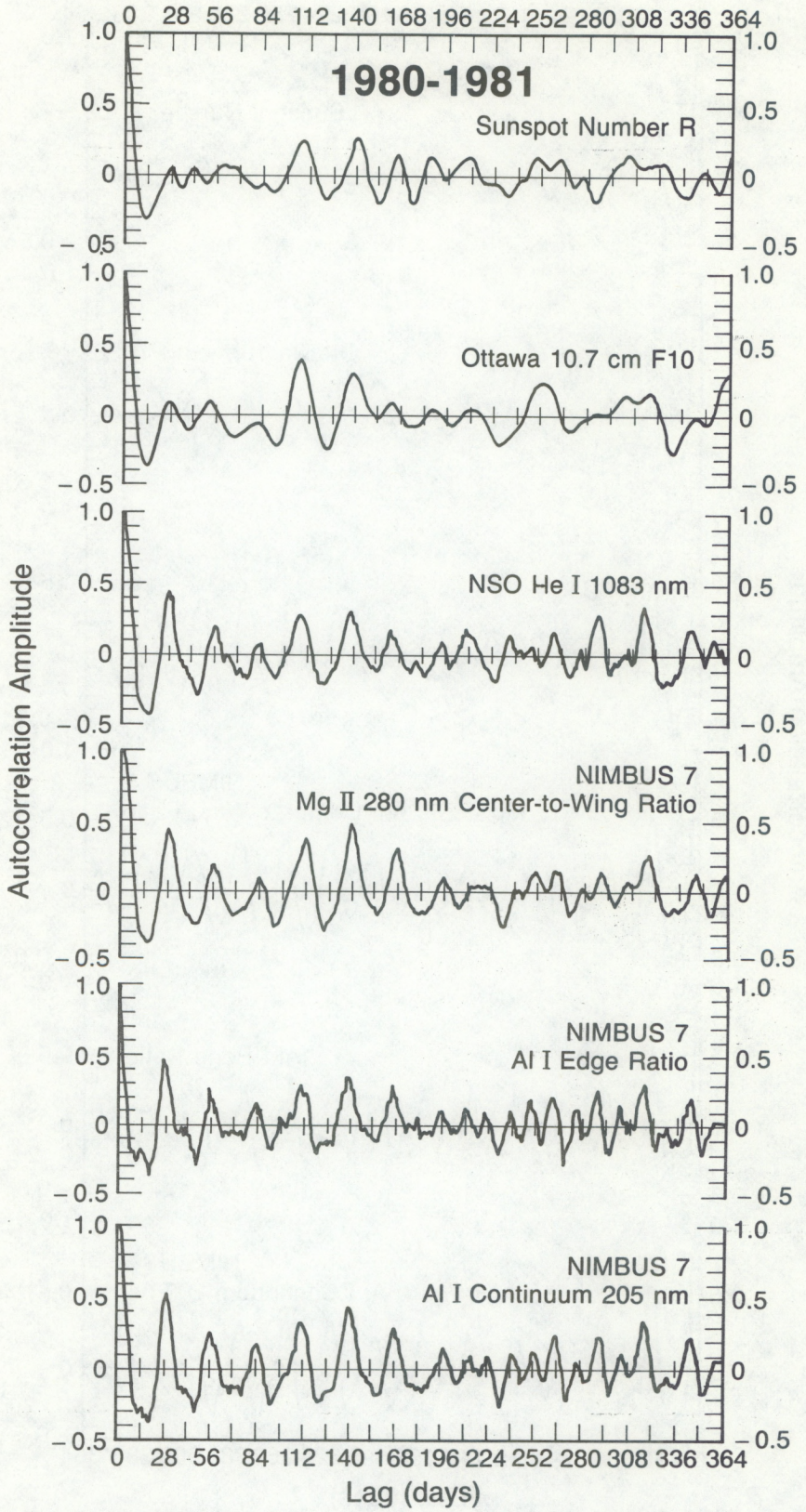

Figure 3.6 Autocorrelation functions for representative UV measurements and ground-based measures of solar activity for 1980 - 1981.

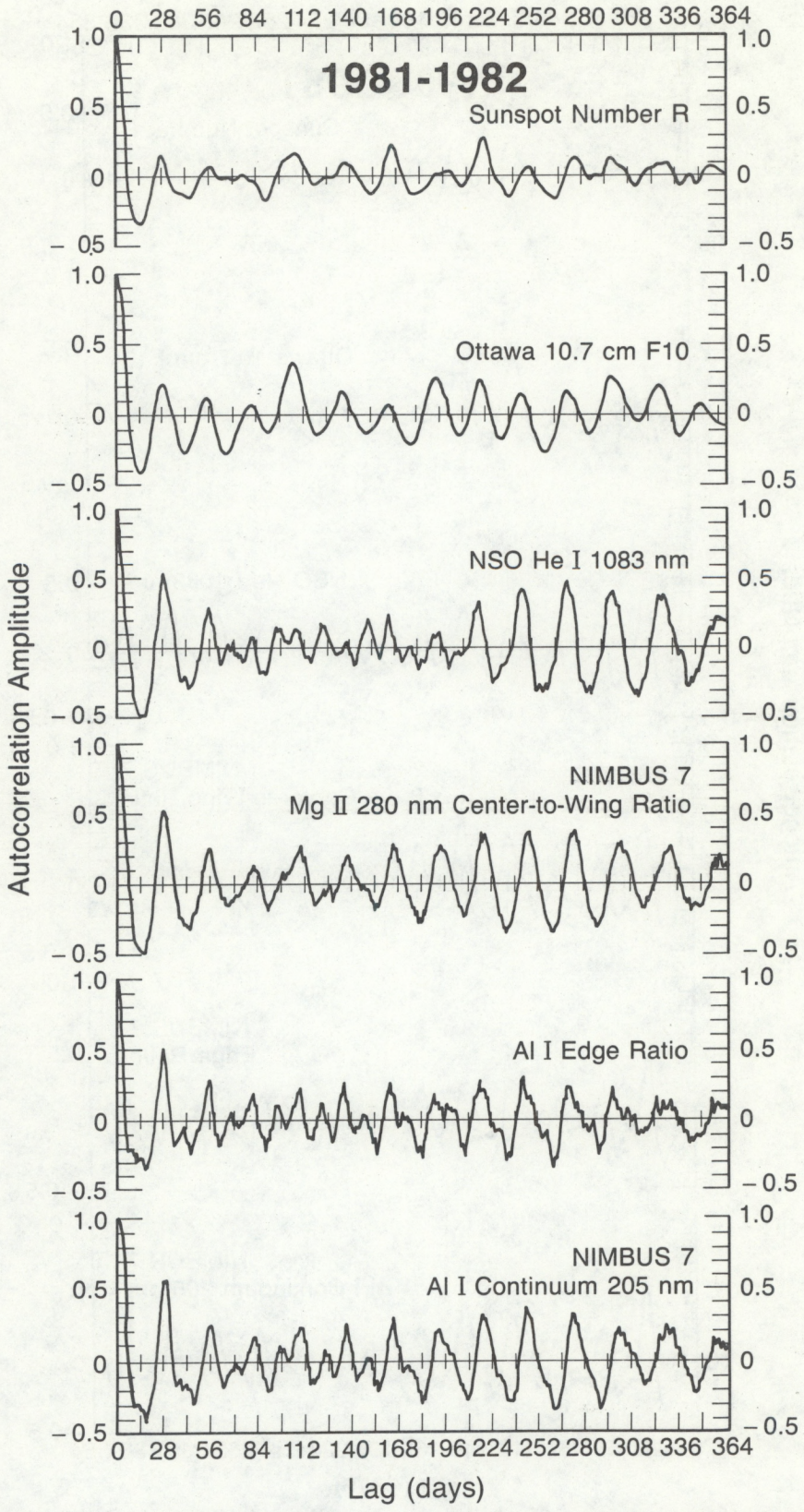

Figure 3.7 Autocorrelation functions for representative UV measurements and ground-based measures of solar activity for 1981 - 1982.

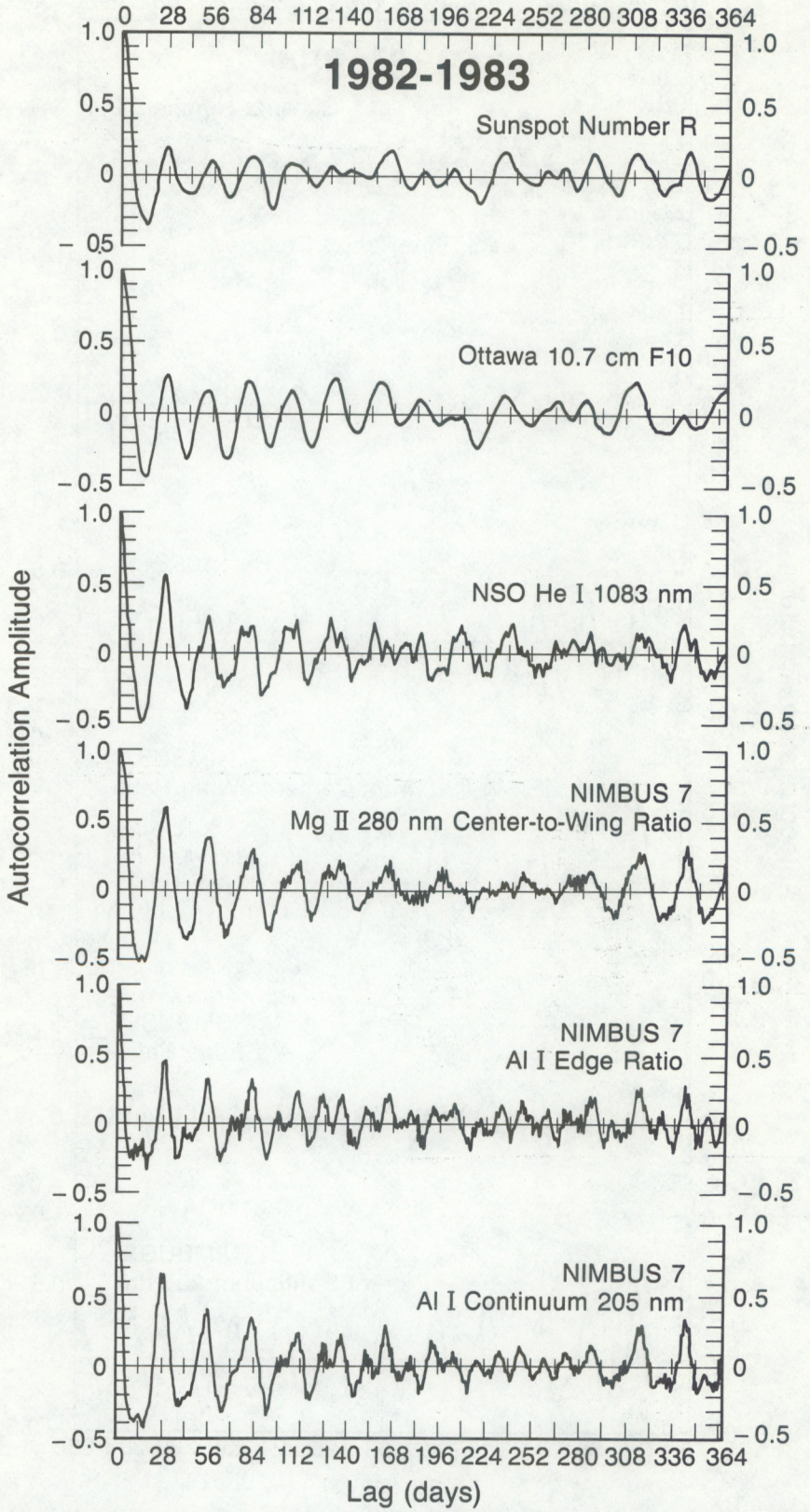

Figure 3.8 Autocorrelation functions for representative UV measurements and ground-based measures of solar activity for 1982 - 1983.

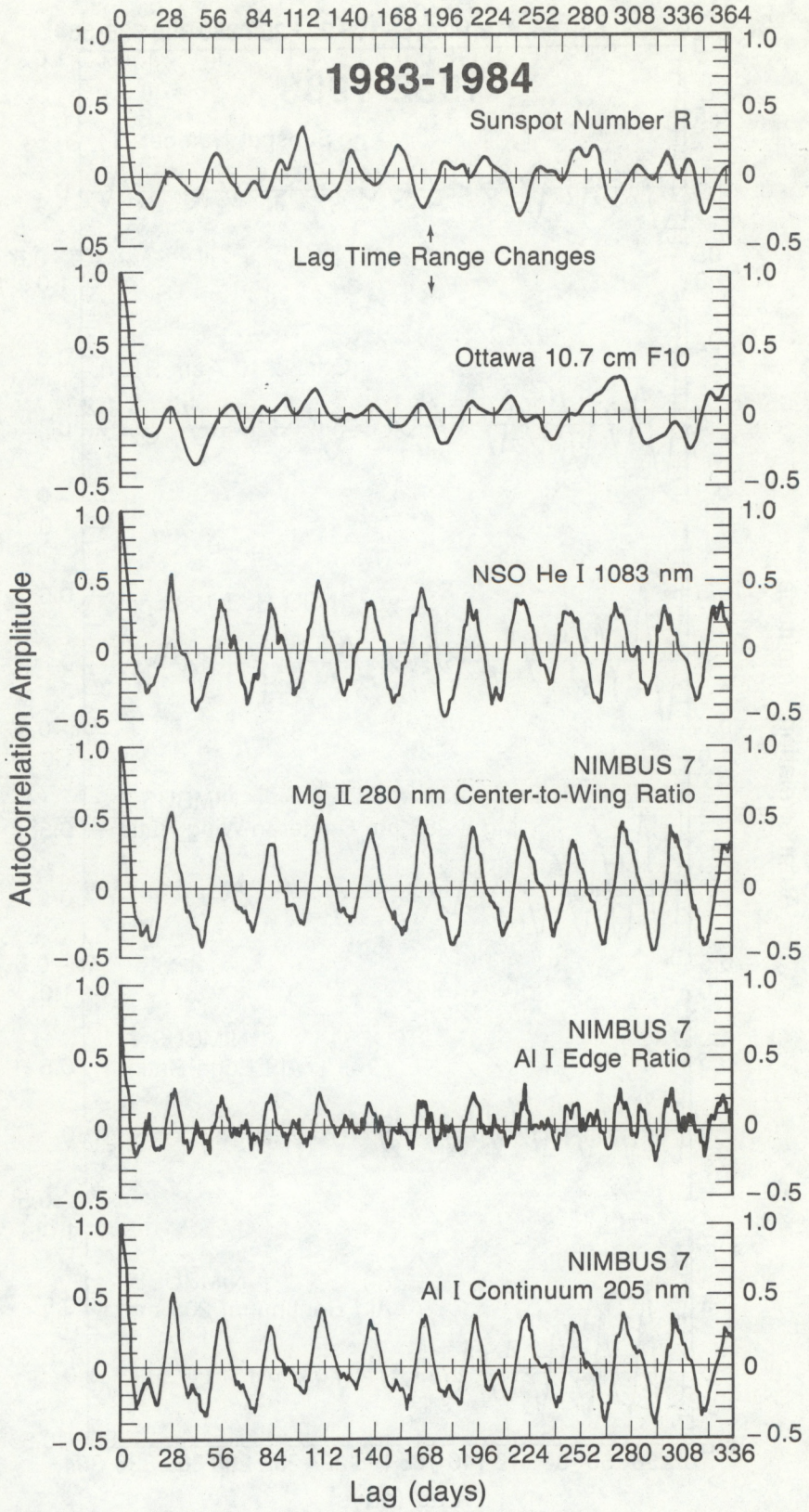

Figure 3.9 Autocorrelation functions for representative UV measurements and ground-based measures of solar activity for 1983 - 1984.

long-term variations, its short term variations closely match those of the UV flux at the center of the line. Note the close similarity between AF for the ground-based measurements of the chromospheric absorption line at 10830 A and that for the Mg II center-to-wing ratio in Figure 3.5 and the close similarity in Figure 3.4 for this same time interval between the 10830 A result and the chromospheric H Lyman beta data. This is our first evidence in this report for a good connection between Heath's UV index and the chromospheric EUV emissions. There are small differences among these three AF curves (Mg II, 10830 A and H Lyman beta) that we interpret as being less significant than some small differences between the bottom three curves in Figures 3.5 - 3.9 that are discussed below. The reason is that in the case of the bottom three curves, the measurements are all from the same satellite, from the same time of day and occurring on the same dates, i. e. missing data occur at the same time. Consequently, small differences are more likely to signify real differences in the temporal characteristics of the solar flux. In the case of comparing Mg II, 10830 A, and H Lyman beta, each of these sets of measurements came from different sources. The measurements were usually made at different times of the day, where the flux variation during a day is usually not large but is still large enough to cause some of the small differences among the three autocorrelation curves. The dates when data were missing and the nature of observational noise differ among these three data sets. Therefore, small differences among their autocorrelation functions do not necessarily signify real differences in their solar fluxes.

3.3 Differences in Short-Term Variations of the Al I Edge Ratio

Compare the three bottom curves in Figures 3.5 - 3.9. Obviously the results for the Al I edge ratio differ from the other two UV cases, especially in Figure 3.9. Note the tendency for minor peaks at odd integer multiples of 14 days in AF for the edge ratio. The 28-day peaks tend to be lower than in the other two UV cases and there is more fine structure in AF for the edge ratio. The fine structure is probably due to a lower signal to observational noise ratio in R(AlI) as was discussed in section 1.4 and in the discussion of Figure 2.6. The peaks near 14-days will be discussed further in Chapter 5. Recall that AF for the photospheric 205 nm flux was shown to be very similar to AF throughout the 170 - 260 nm range. This means that we know the Al I edge ratio has significant differences in short-term variations with respect to those of the UV flux important to the stratosphere. Returning to the Mg II ratio, while its AF is more similar to that for 205 nm than all the other curves in Figures 3.5 - 3.9, there are some slight differences mainly in the first four valleys. This difference is related to the lower strength of 13-day periodicity that will be discussed further in Chapter 5.

3.4 Persistence of Solar Rotational Variations

Donnelly et al. (1986b) and Donnelly (1987) used the average of the first four solar rotational peaks in the autocorrelation as a quantitative measure of the persistence of the solar rotational modulation. Actually, the average was multiplied by ten and rounded to one significant integer and labeled PSVR, for persistence of solar rotational variations, i. e.

$$PSRV = 10[AF_{max}(\sim 28 \text{ days}) + AF_{max}(56\text{days}) + AF_{max}(84) + AF_{max}(112)]/4 \quad (9)$$

For EUV wavelengths, PSRV varied greatly from wavelength to wavelength as the source region varied from hot corona ($T > 3 \times 10^6$ ^oK) , cool corona ($T < 2 \times$

10^6 ^oK), transition region, base of the transition region and upper chromosphere and chromosphere. Donnelly (1987) concluded that high persistence of solar rotational variations was caused by the major episodes of solar activity, where the UV flux rose to its highest rotational peak usually on the second rotation rather than on the first rotation (and sometimes on the third rotation) and then slowly decayed on the subsequent several solar rotations. An outstanding example of this is shown in Figure 2.4, in the episode starting in June and running across the rest of the figure. Examples of such episodes include the following: (a) starting in late August 1979, in Figure 1 of Donnelly et al. (1982), (b) starting in November 1979 in Figure 3 of Donnelly et al. (1986a) and (c) starting in June 1982 in Figure 3 of Donnelly et al. (1983).

In the case of the solar UV flux, the persistence results are very uniform, so the use of more than one digit is necessary. Here we have defined the persistence as PSRM, for persistence of solar rotational modulation as PSRM = PSRV/10, or

$$PSRM = [AF_{max}(\sim 28 \text{ days}) + AF_{max}(56\text{days}) + AF_{max}(84) + AF_{max}(112)]/4 \qquad (10)$$

Figure 3.10 shows this revised persistence function for 1979 - 1980. The corresponding results of Donnelly (1987) for EUV wavelengths and this same time interval range from about 0.11 for hot coronal 1 - 8 A soft X-rays, 0.21 for hot coronal EUV lines, like Fe XV 28.4 nm and Fe XVI 33.5 nm, 0.36 for cool coronal Fe XIII near 20 nm, 0.20 for transition-region Fe XI near 18 nm, 0.11 for transition-region Fe IX near 17 nm, 0.29 for upper-chromospheric He II at 30.4 nm, 0.38 for chromospheric He I at 58.4 nm and H Lyman alpha at 121.6 nm, and 0.39 for chromospheric H Lyman beta at 102.6 nm. Thus the persistence is higher at most UV wavelengths than for EUV wavelengths. The chromospheric EUV results fall in the range 0.29 to 0.39, which is in good agreement with the UV chromospheric results, namely Si II near 182 nm (background continuum removed), and the Ca H and Ca K lines, where the Mg II 280 nm result has even higher persistence.

The main result in Figure 3.10 is that the persistence is very high (near 0.5) and fairly uniform for UV wavelengths in the 170 - 260 nm range and the Mg II and I lines. Solar indices like the 10.7 cm flux F10, the sunspot number R and the Ca-K plage index (0.25, not shown) have much lower values of persistence. The PSRM values for 160 - 165 and 165 - 170 nm are lower than for most wavelengths in the 170 - 260 nm range. We interpret this as being caused partly by more chromospheric emissions at these wavelengths, where the persistence for chromospheric fluxes tends to be slightly lower than for the photospheric UV fluxes, and partly from the ratio of solar signal to observational noise being smaller at these wavelengths. The latter is caused by the solar flux at these wavelengths being much lower and the noise higher near this end of the spectrometer wavelength range than at 170 nm and longer (See Figure 1.1).

Figures 3.11 - 3.14 show similar results for the other two-year intervals studied. The 5 nm wide bars are fairly level in persistence from 170 to 260 nm in each figure but the level varies from figure to figure according to the particular episodes of major activity included in the respective two-year interval. In Figures 3.10 - 3.14, the level of the persistence at 205 nm, (which is in the solar Al I continuum absorption region) lies in the middle of the persistence level of the 5 nm bars from 170 - 260 nm. Therefore, we used

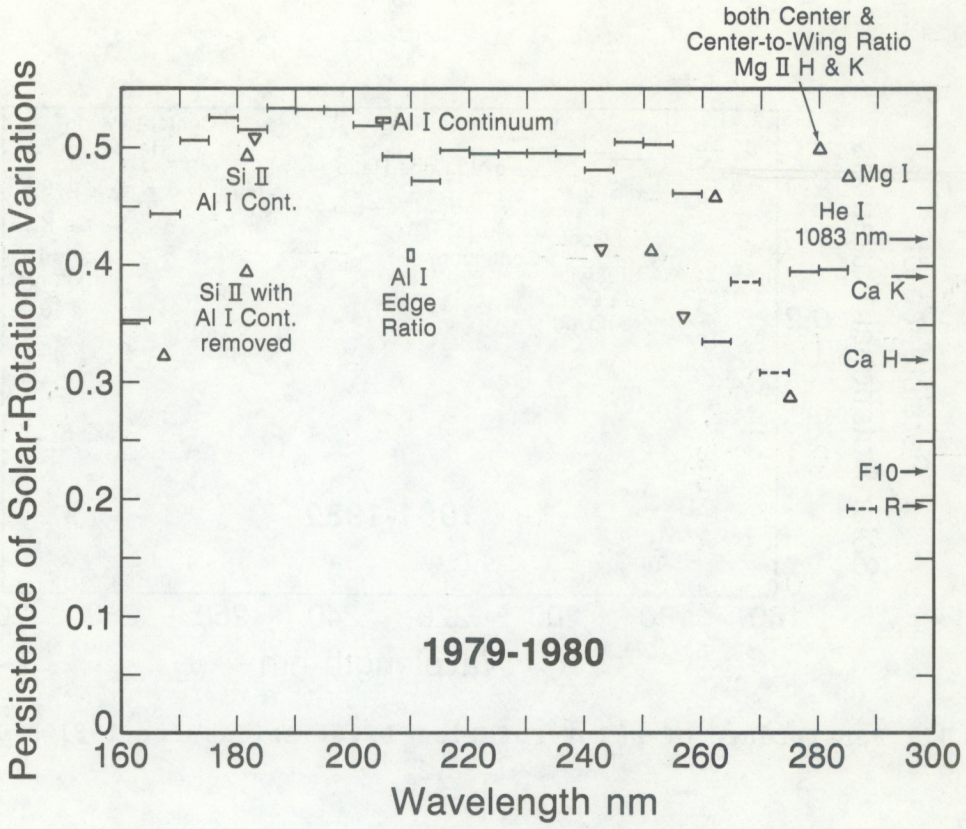

Figure 3.10 Persistence of solar-rotational variations for 1979 - 1980.

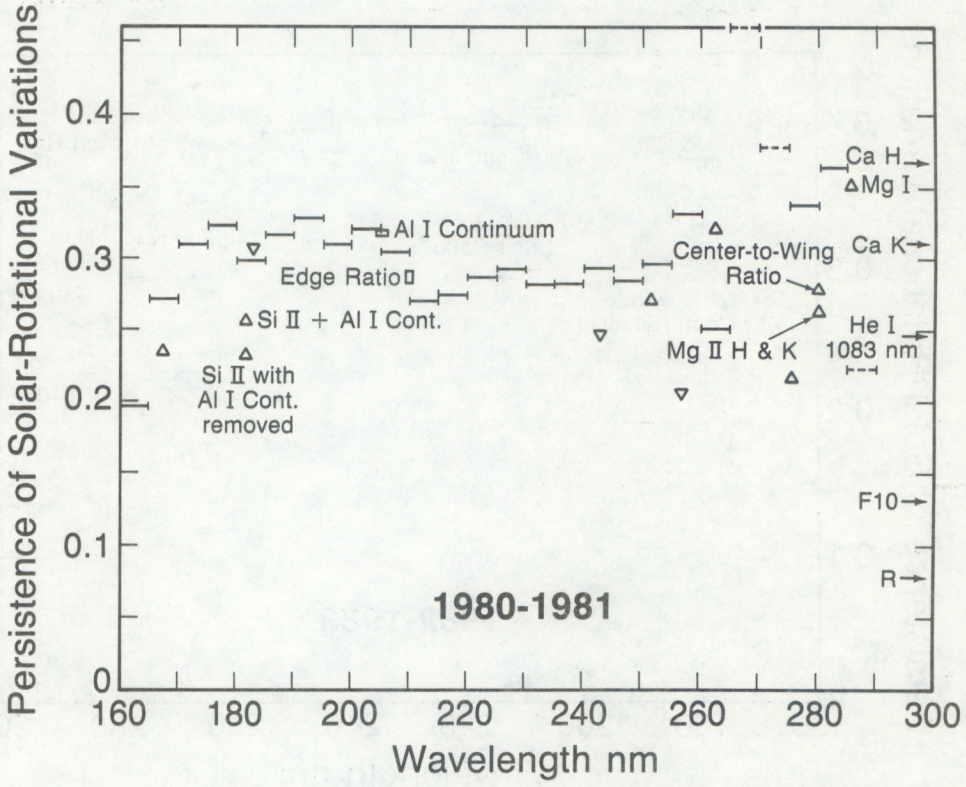

Figure 3.11 Persistence of solar-rotational variations for 1980 - 1981.

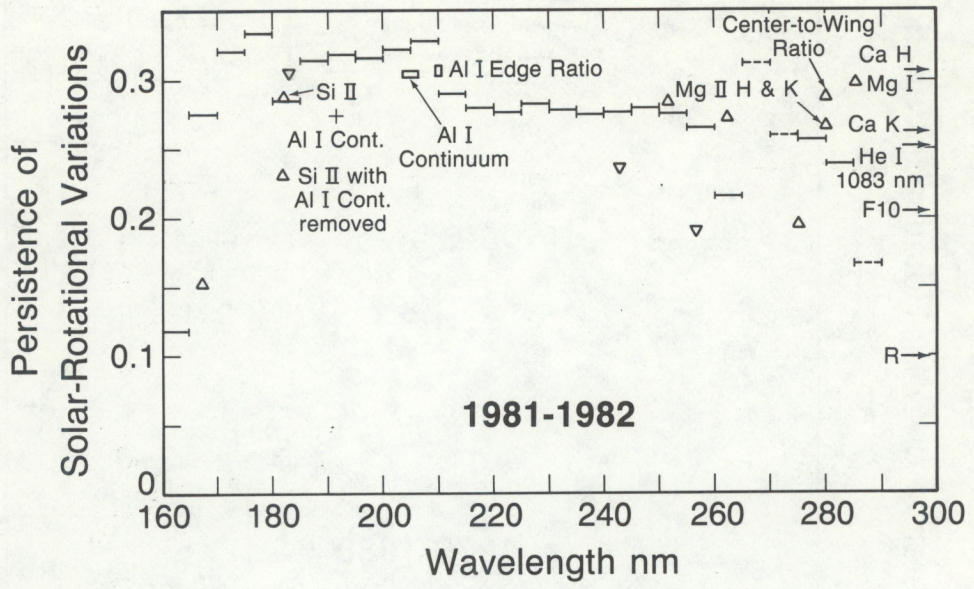

Figure 3.12 Persistence of solar-rotational variations for 1981 - 1982.

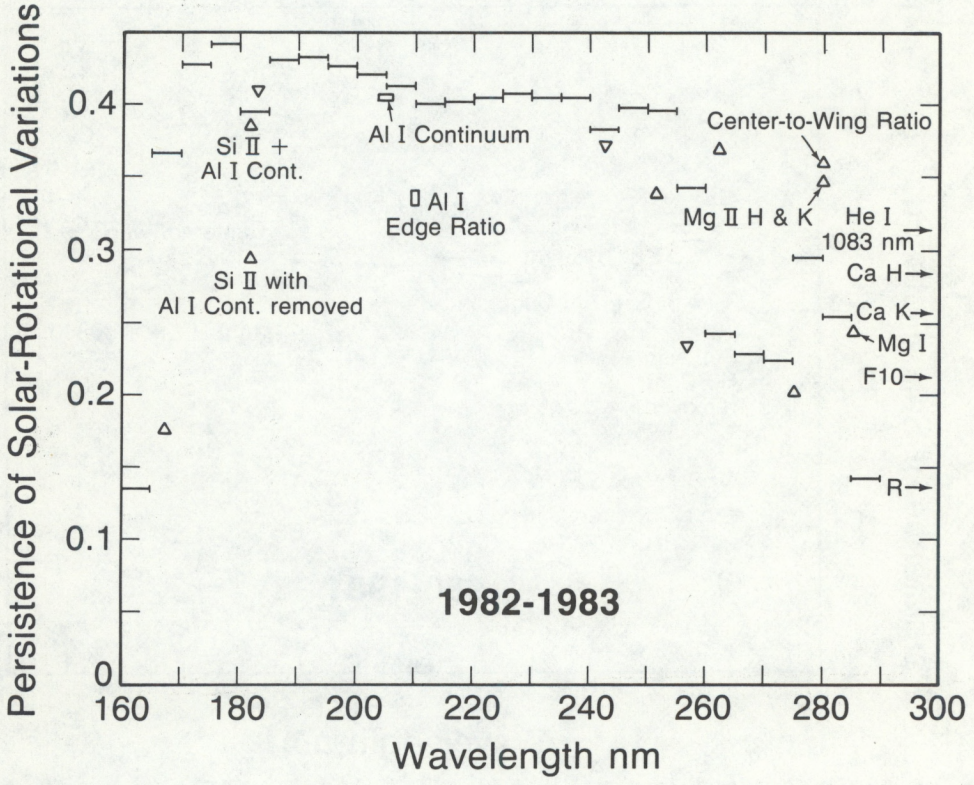

Figure 3.13 Persistence of solar-rotational variations for 1982 - 1983.

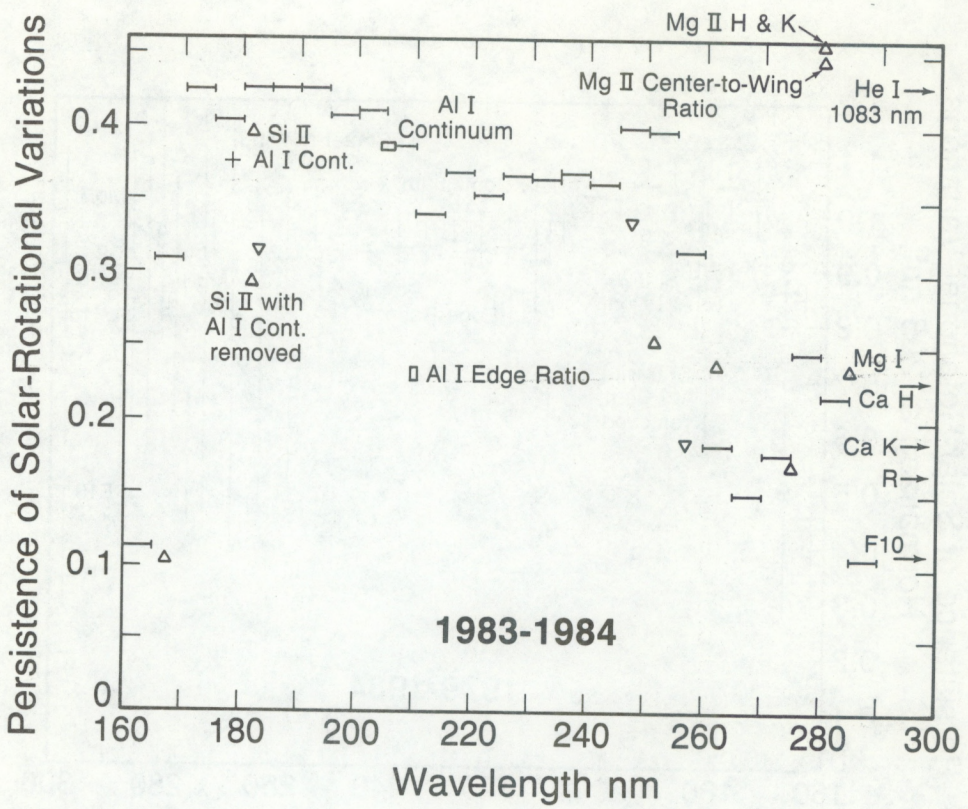

Figure 3.14 Persistence of solar-rotational variations for 1983 - 1984.

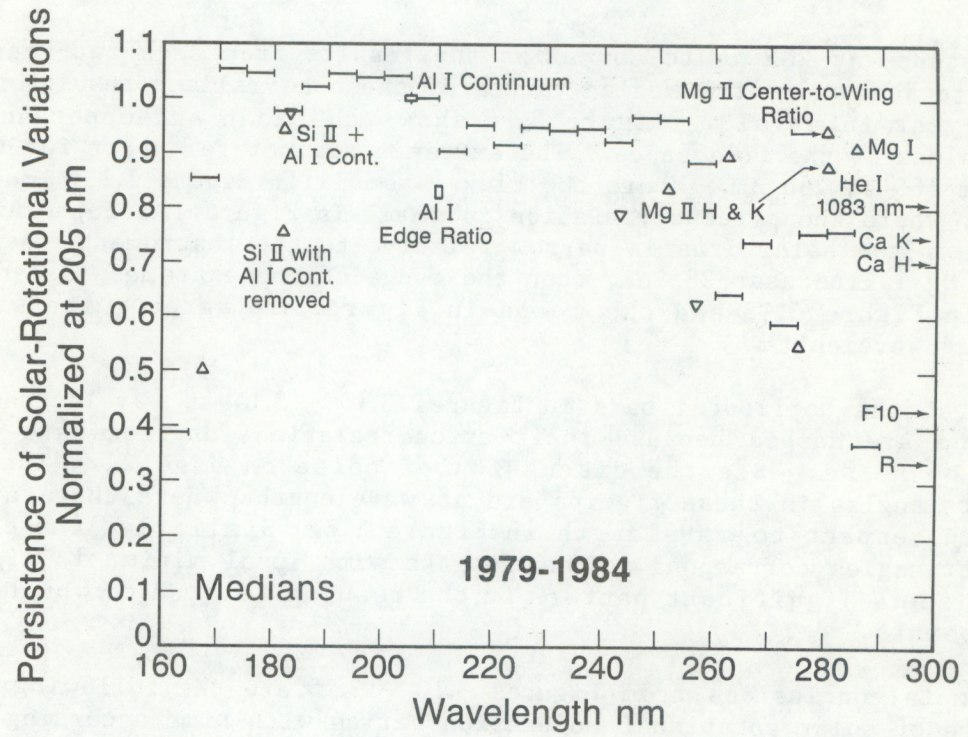

Figure 3.15 Median persistences for 1979 - 1984.

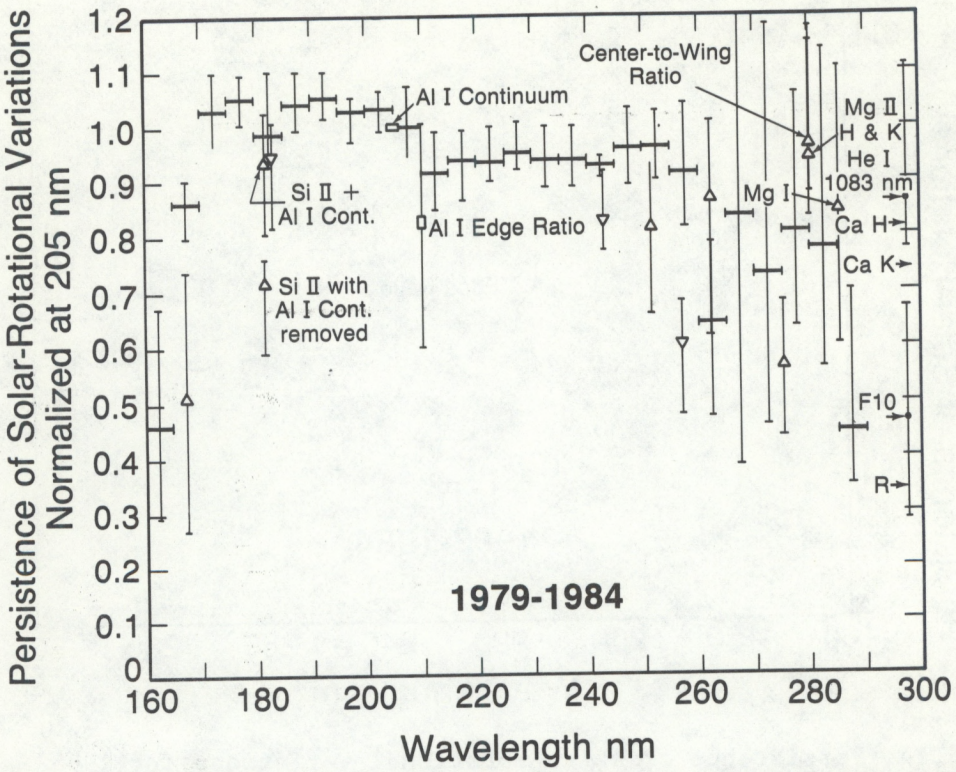

Figure 3.16 Means and extremes of persistence for 1979 - 1984.

the persistence at 205 nm to normalize the results from each two-year interval. Figure 3.15 shows the median values of these normalized results from the five two-year intervals. Figure 3.16 shows the mean and upper and lower extreme values of the five cases. The extremes are not far apart for the 5 nm bands from 165 to 265 nm. Where the flux is small in Figure 1.1, namely 160 - 165 nm, or where the percent variation is small in Figure 1.2, for example 265 - 275 nm, or the solar line is narrow relative to the instrument's bandwidth, as in the Mg I line near 285 nm, then the range of the extremes is large. The medians in Figure 3.15 and the means in Figure 3.16 agree quite well as a function of wavelength.

Some of the horizontal bars in Figures 3.10 - 3.14 at wavelengths longer than 265 nm are dashed because their autocorrelation functions are strongly affected by noise. See the discussion of noise on page 21. The upward pointing triangles in these figures are at wavelengths where there are local peaks with respect to wavelength in Figure 1.2. Similarly, the downward pointing triangles correspond to wavelengths with local minima in Figure 1.2. We do not see a significant pattern in the results related to which way the triangle points.

Our main conclusions from Figures 3.10 - 3.15 are the following: (1) the persistence of solar rotational modulation varies with time according to what episodes of major activity occur within the time interval studied, (2) the relative wavelength dependence is fairly uniform especially for most wavelengths in the 170 - 260 nm range, where the UV radiation changes within that range dominate the induced stratospheric variations in ozone density and

temperature changes, (3) persistence for the Al I edge ratio tends to be lower on average and more variable than for most wavelengths in the 170 - 260 nm range, (4) the persistence in the Mg I continuum range of 210 - 255 nm tends to be level but about ten percent less on average from the level in the Al I continuum at 170 - 205 nm, (5) the persistence for the fluxes in the 160 - 165 nm range, the Si II lines, F10 and R tend to be much lower than in the 170 - 260 nm range, (6) the persistence of the Mg II center-to-wing ratio tends to be slightly higher but in close agreement with that for the center-of-line flux, and both agree well on average with the persistence in the Mg I continuum at 210 - 255 nm, and (7) compared to the large variations in persistence for various EUV emissions, the persistence of solar-rotational modulation is very high and uniform for UV radiation in the 170 - 260 nm wavelength range.

4. CROSS CORRELATION ANALYSES

Figure 4.1 shows a typical example of the cross correlation results for the short-term residuals of UV fluxes and ground-based measures of solar activity with respect to the short-term residuals of the 205 nm flux. In each frame, the dashed curve is the autocorrelation function (AF) for the 205 nm flux, which by definition is symmetric about the zero lag line. The closer the temporal variations of the comparison data set in the cross correlation function (CCF) are in shape to those of the reference 205 nm data, the closer the solid cross correlation curve is to the dashed autocorrelation curve. In the case of the 5 nm bands, 175 - 180 and 250 - 255 nm, the solid curve essentially covers the dashed curve and the curves are very symmetric. Similar results occur for all the other 5 nm bands in the 170 - 260 nm range. CCF for the Si II emission lines near 182 nm, the Mg II h & k absorption lines near 280 nm and the Mg I absorption line near 285 nm, each with respect to the 205 nm data, also are a fairly close match to the 205 nm AF. The results for the other two-year intervals likewise showed symmetrical and AF-matching cross correlation curves for the NIMBUS-7 solar UV flux measurements. Since the 27-day solar rotational variations dominate the AF and CCF curves, we conclude that the CCF results show that the shape of the short-term temporal variations of solar UV flux (170 - 285 nm) is very uniform with respect to wavelength, although the magnitude of these variations varies with wavelength (Figure 1.2).

The results for the mountain-top measurements of the chromospheric He I absorption line near 10830 A differ noticeably with the 205 nm AF. However, these measurements are made at different times of the day and usually have missing data on different days, which certainly contributes part of the differences between the CCF and the 205 nm AF. Note the slight asymmetry to the left in the CCF for 10830 A, which is a consistent result with respect to those for other time intervals (Donnelly et al., 1985, 1986b), except for close symmetry for the 1980-1981 interval. We suggest this asymmetry may be a consequence of the 10830 A He I data being from the top of the chromosphere with some influence from the overlying corona while the 205 nm flux is from the upper photosphere and lower chromosphere.

The CCF's for the sunspot number R and the Ottawa 10.7 cm solar radio flux F10 are strongly asymmetric to the left, which has previously been interpreted as being a consequence of R and F10 rising faster, peaking earlier and decaying faster than the photospheric UV flux during an episode of major activity (Donnelly et al., 1985). The main new result here is that this strong asymmetry for F10 and R versus the UV flux is a consistent result throughout the six years of data studied.

The CCF results for the Mg II center-to-wing ratio are like those for the center of the line shown in Figure 4.1, i. e. a close match for 27-day rotational variations. The CCF results for the Al I edge ratio are also a fairly good match to the 205 nm AF, where the biggest differences occur in the valleys, which is related to 13-day periodicity. That is shown more directly in the next chapter.

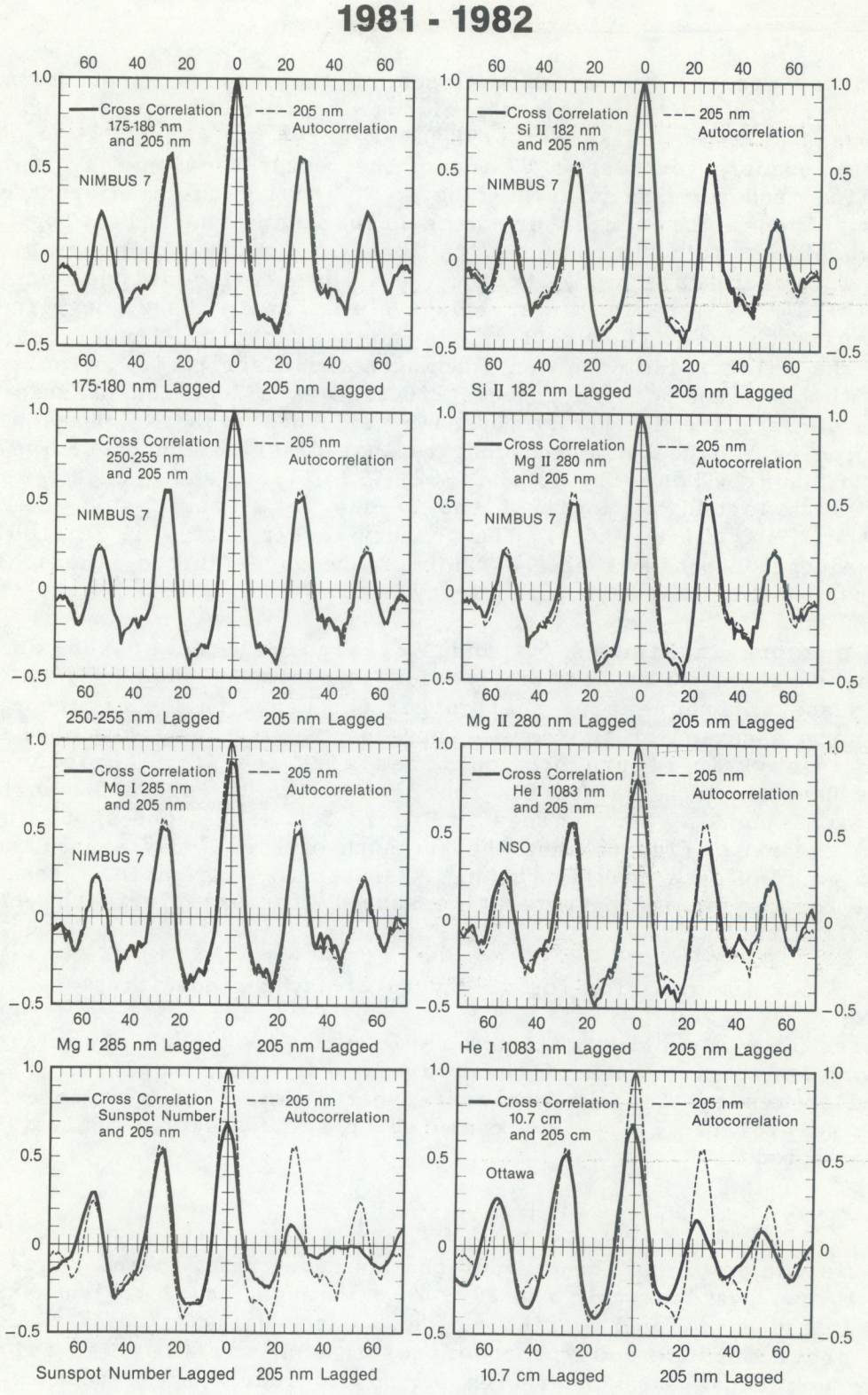

Figure 4.1 Cross-correlation functions for representative UV wavelengths and ground-based measures of solar activity.

5. POWER SPECTRA ANALYSES

5.1 Example Power Spectra

The power spectra and other analyses of the residual short-term variations used here are the same as those discussed in Chapters 4 - 7 of Heath et al. (1984) and by Lean and Repoff (1987). Figures 5.1 and 5.2 show examples of the power spectra for Heath's UV index, the center-to-wing ratio for the Mg II h & k line, and for the solar UV flux at 205 nm for three adjacent two-year intervals. The main features of these figures are the following: (1) the major power line is in the range 27 to 28 days, (2) the secondary line is in the range 13.4 to 14 days periodicity, (3) a low level continuum and (4) the power in the 14-day line is larger relative to that in the 27 day line in the 205 nm results than for the Mg II center-to-wing ratio. The 27-day line is caused by the solar rotation of an inhomogeneous distribution of solar active regions with one main peak in its distribution as a function of solar longitude. The 14-day line is mostly caused by episodes with two peaks per rotation produced by two peaks in the longitudinal distribution of active regions roughly 180^{o} apart (Donnelly et al.,1982, 1983, 1985) and only a small part results from a second harmonic of the 27-day variation that is related in phase to the 27-day fundamental. The primary result that will be studied here is the wavelength dependence of the ratio of the power in the line at 13 to 14 days to that at 27 to 28 days periodicity.

Each spectra in Figures 5.1 and 5.2 is normalized so the sum of the percent power values is 100%, where the sum is over each frequency in the grid of equally spaced frequencies that covers the range in the figures and also extends out to a period of two days. Consequently, the presence of a stronger line near 14 days in Figure 5.2, combined with the normalization of each spectra, causes the peak values for the 27-day line in Figure 5.2 to be lower than the corresponding peak values in Figure 5.1. Hence, one should **not** conclude from these two figures that the strength of the 27-day signal is weaker in the 205 nm flux data than in the Mg II center-to-wing ratio. These spectra are useful for comparing their relative shapes, for example in the 13 to 27-day power line ratio.

5.2 Power Ratios for 13-day to 27-day Periodicities

Figures 5.3 - 5.7 illustrate the ratio of 13 to 27-day power as a function of wavelength for each of the two year intervals studied. Figure 5.8 shows similar results for the whole six year interval of available NIMBUS-7 data. The power ratio $P_{13/27}$ was computed from the spectral analysis results from the equation

$$P_{13/27} = [P_{13} - P_b]/[P_{27} - P_b], \qquad (11)$$

where P_{13} is the power at the peak of the spectral line in the range 13 - 14 days, P_{27} is the peak power in the 27 - 28 day range, and P_b is an estimate of the power in the background continuum, which was usually taken as the power at 11.9 days providing the power for periods in that vicinity was fairly constant. The horizontal bars in Figures 5.3 to 5.8 indicate the results for the UV flux averaged over 5 nm. When the spectral shape was very noisy and the estimate of the background power was difficult to determine accurately, a dashed bar is shown. Upward pointing triangles are at wavelengths where the results in Figure 1.2 are local peaks, and vice versa the downward pointing

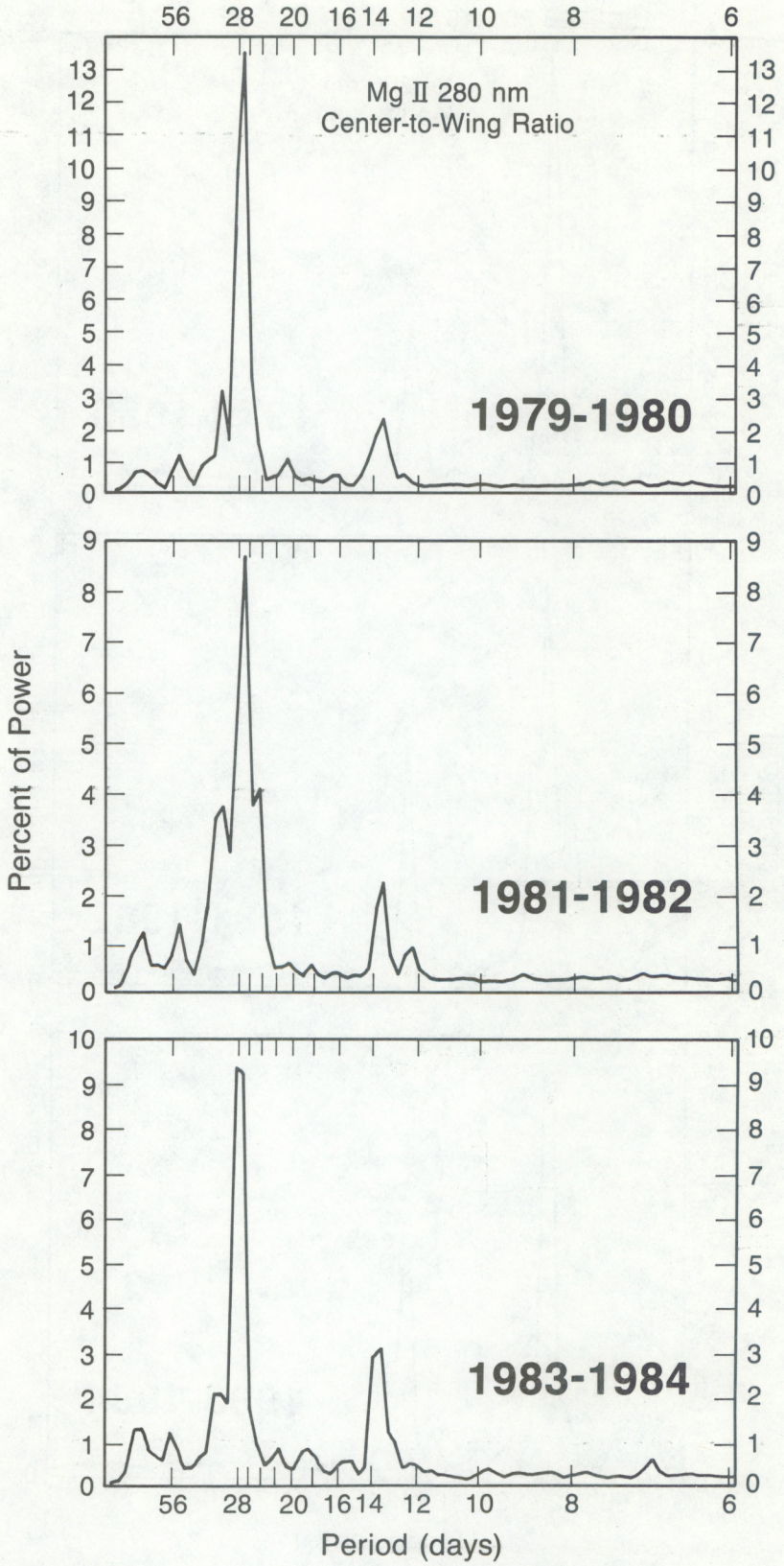

Figure 5.1 Power spectra for the center-to-wing ratio of the MgII h & k lines.

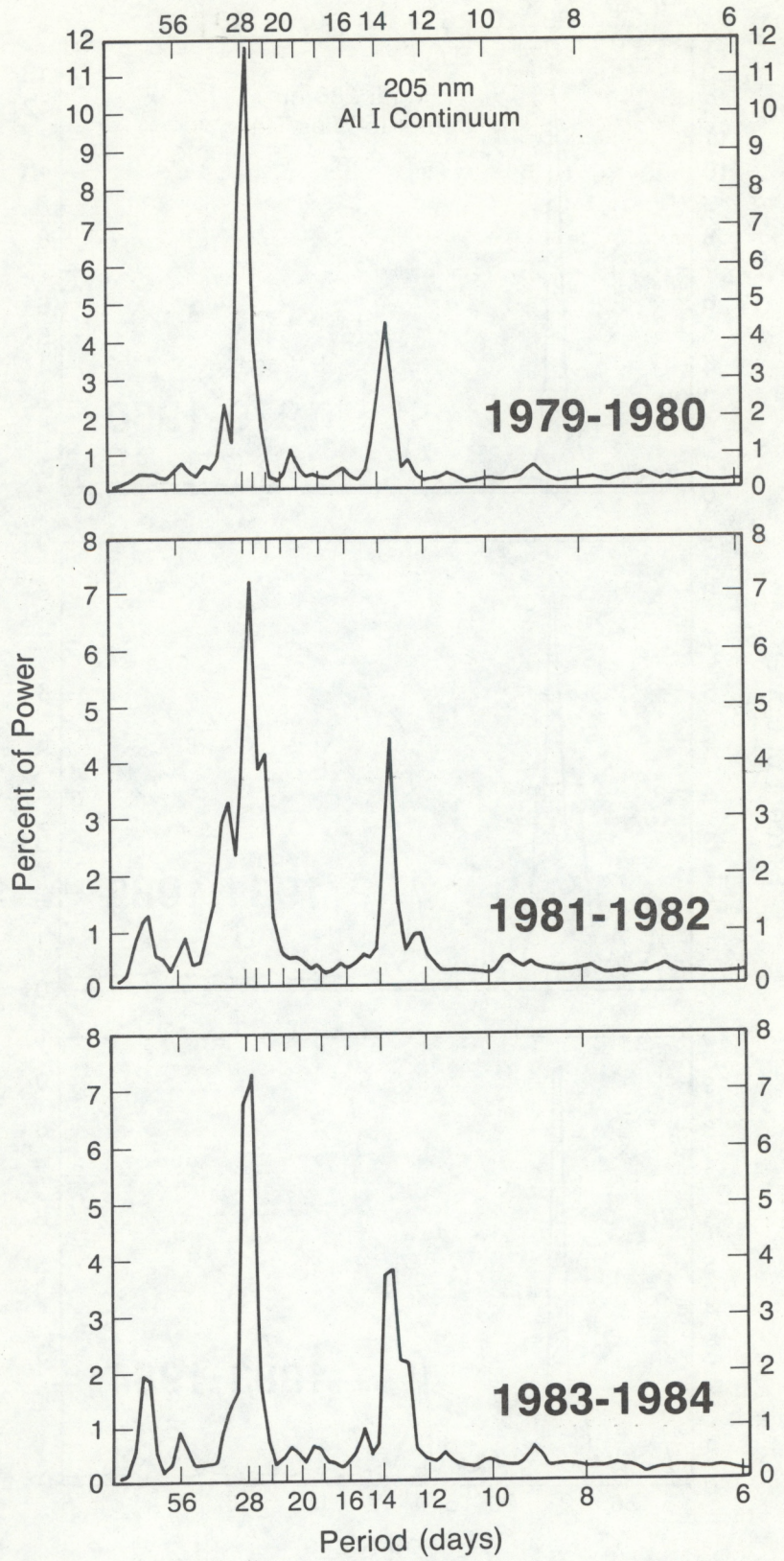

Figure 5.2 Power spectra for the NIMBUS-7 measurements of the 205 nm flux.

triangles are local minima in Figure 1.2. The triangle at the right side of Figures 5.3 - 5.8 and marked "Mg I" is the Mg I absorption line at 285 nm, which can be seen in Figure 1.2 as the small enhanced line to the right of the very strongly enhanced Mg II h & k lines combined at 280 nm. The horizontal rectangle labeled "Al I continuum" corresponds to the power ratio results for the UV flux at the single wavelength setting of 205 nm, which is in the solar Al I absorption continuum.

The power ratio for any particular wavelength varies from one figure to another according to what episodes of 13-day periodicity and other episodes of 27-day periodicity occur in a particular time window. Common relative features as a function of wavelength in Figures 5.3 - 5.8 include the following: (1) low power ratios for 160 - 165 nm, (2) lower at 180 - 185 nm than for the adjacent 5 nm bins, (3) high values for 175 - 180 and 185 - 260 nm, the Mg I line and the flux in the Al I continuum at 205 nm, and (4) medium values for the Mg II lines. Normalization of the five two-year cases to their respective power ratios at 205 nm produced the average summary results shown in Figures 5.9 and 5.10, where the tips of the vertical range markers in the latter figure mark the extremes among the five normalized cases. The median and mean values agree quite well and consitute our best knowledge of the relative wavelength dependence of the average normalized 13- to 27-day power ratio, where the average ratio at 205 nm for Figures 5.3 - 5.7 is 0.49, which agrees well with the 0.47 value in Figure 5.8.

5.3 EUV Power Ratios

The 13- to 27-day power ratios have been shown to depend on the location of the time window used, and are therefore also dependent on the width of the window. Furthermore, these results are affected by the way the data were filtered (twelfth-order polynomial detrended in our analyses), missing data handled and power spectra computed (autocorrelation estimation). Consequently, the 13- to 27-day power ratios from two different studies should usually not be compared. However, the EUV results in Figure 5.1 of Donnelly et al. (1986b) can be compared with the results in Figure 5.3 because the filtering and analysis techniques used, and the width and location (1979 - 1980) of the time window are the same. Most of the chromospheric EUV results have ratios in the range 0.1 to 0.2, which agrees well with the chromospheric Si II and Mg II results in Figure 5.3. The coronal EUV fluxes had ratios in the range 0 to 0.06, quite low indeed. Conversely, the soft X-ray flux has high ratios where the 13-day periodicity is out of phase with that at UV wavelengths because the optically thin X-rays peak when the two groups of active regions separated by roughly 180^{o} in solar longitude are near the solar limbs while the optically thick UV flux peaks when one of the groups is near the center of the sun (Donnelly et al., 1982).

5.4 Ground-Based Measures of Solar Activity

Table 5.1 lists the 13- to 27-day power ratios for three ground-based measures of solar activity, namely the sunspot number (R), Ottawa 10.7 cm flux adjusted to 1 AU (F10) and the equivalent width (EW) of the He I absorption line at 1083 nm measured at the National Solar Obvservatory. These three sets of results show that the power ratios for F10 are usually very low. The

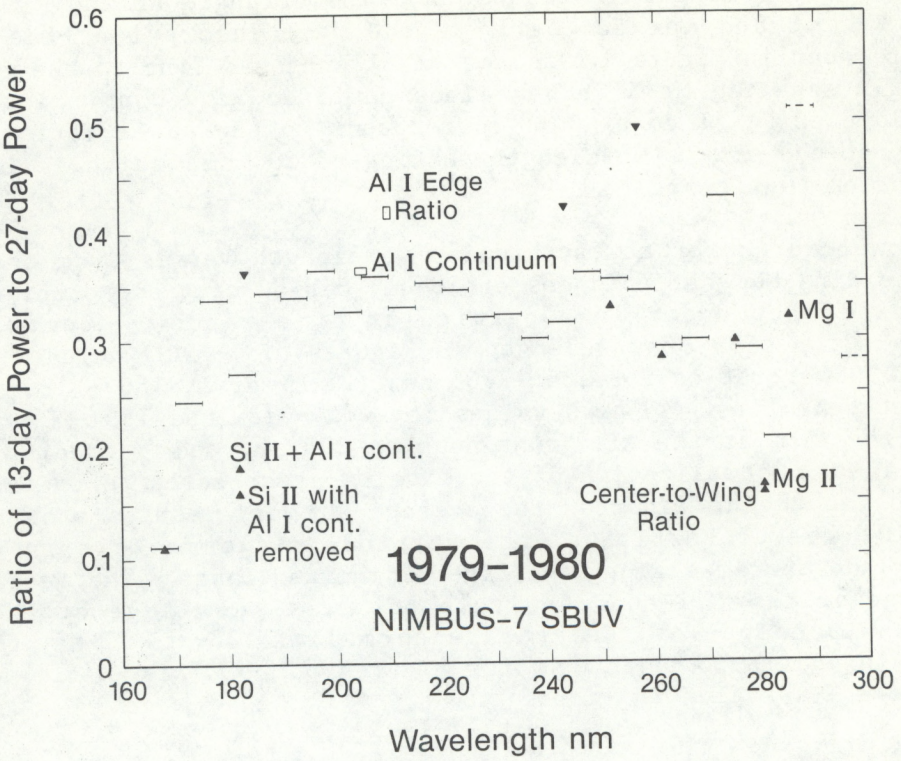

Figure 5.3 Ratio of 13-day power to 27-day power for 1979 - 1980.

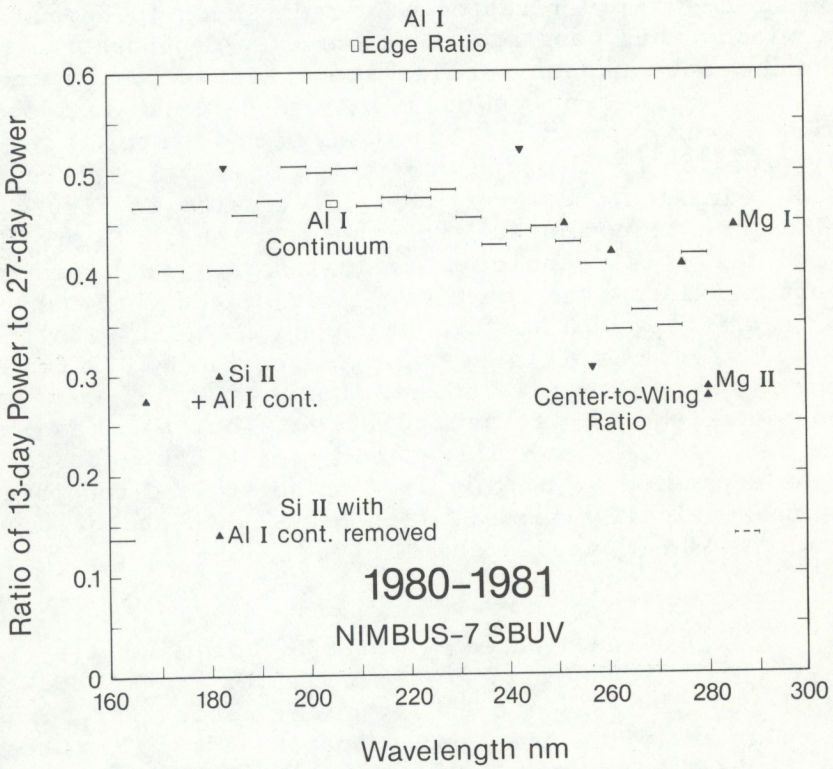

Figure 5.4 Ratio of 13-day power to 27-day power for 1980 - 1981.

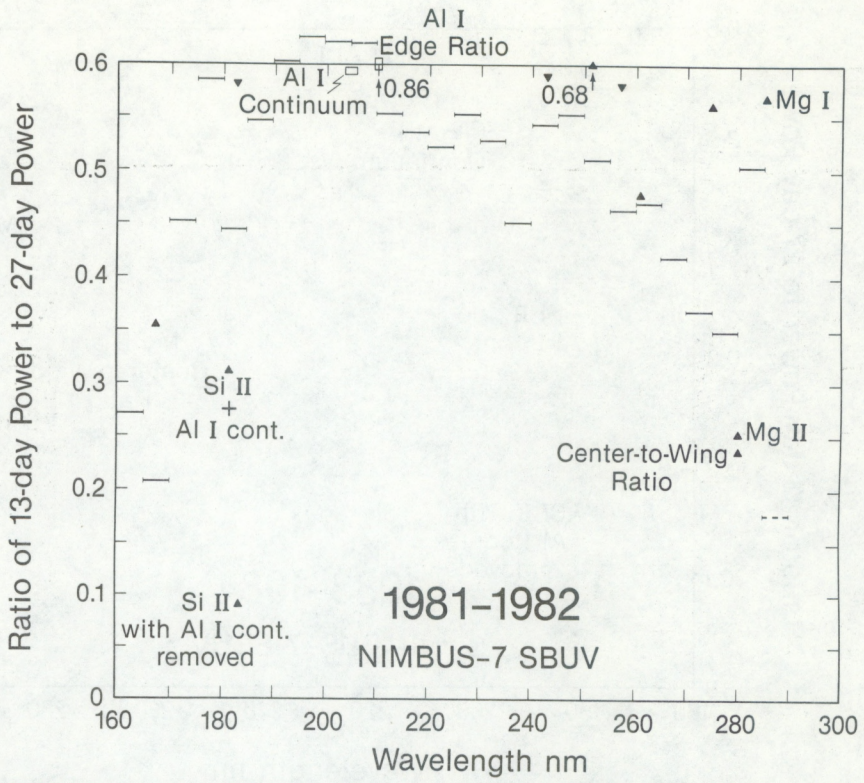

Figure 5.5 Ratio of 13-day power to 27-day power for 1981 - 1982.

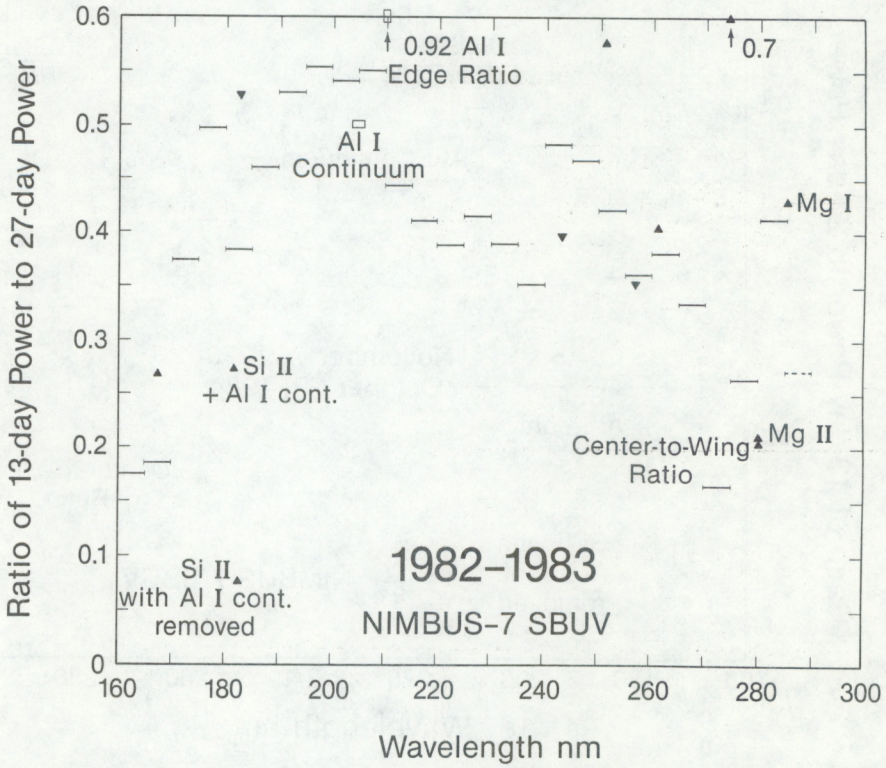

Figure 5.6 Ratio of 13-day power to 27-day power for 1982 - 1983.

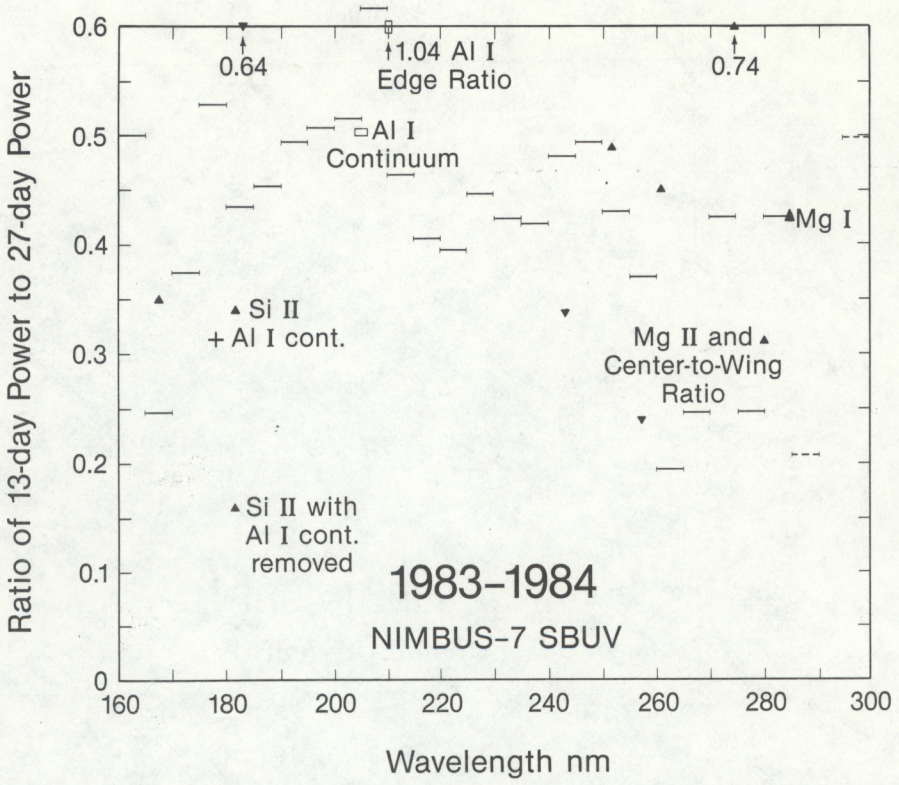

Figure 5.7 Ratio of 13-day power to 27-day power for 1983 - 1984.

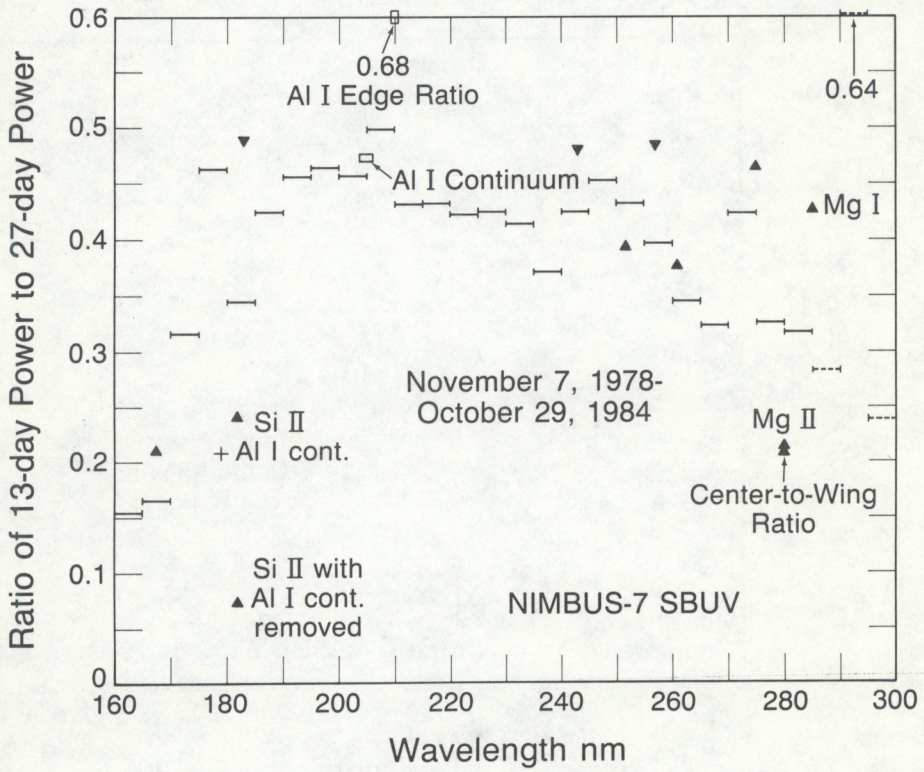

Figure 5.8 Ratio of 13-day power to 27-day power for six years of data.

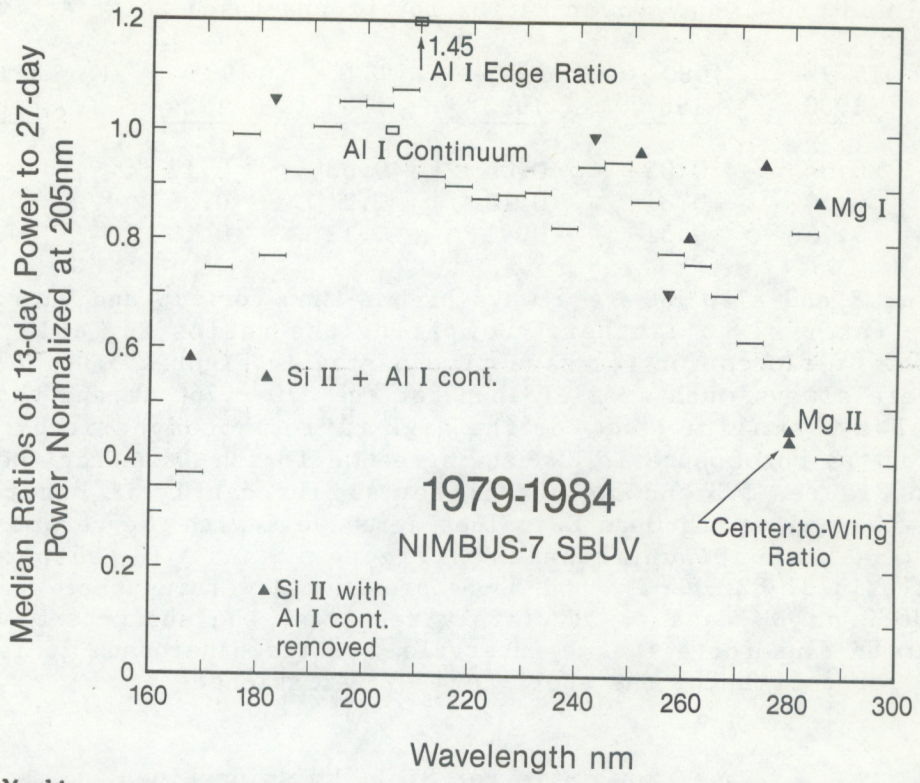

Figure 5.9 Median ratio of 13-day power to 27-day power for 1979 - 1984.

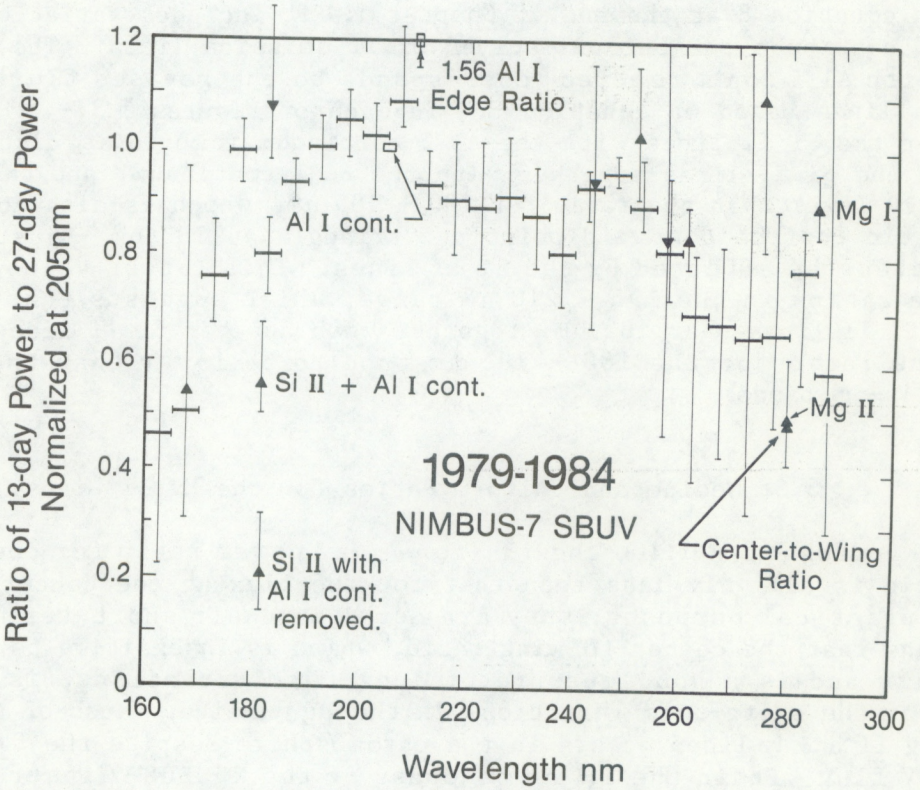

Figure 5.10 Mean power ratios and high and low extremes for 1979 - 1984.

Table 5.1 13- to 27-day Power Ratios for Ground-Based Solar Activity Measures

Solar Data	1979 - 1980	1980 - 1981	1981 - 1982	1982 - 1983	1983 - 1984	Normalized @ 205 nm Median	Mean
F10	0.04	0.05	0.04	0.03	0.17	0.10	0.13
R	0.10	0.31	0.18	0.21	0.36	0.36	0.40
EW	0.15	0.31	0.41	0.12	0.16	0.42	0.46

ratios for R and also EW are always higher than for F10 and vary greatly from one time interval to another. Comparing the ratios in Table 5.1 with the ratios for UV fluxes for the same time period in Figures 5.3 - 5.7, the ratios for F10 are always much smaller than for the 170 - 260 nm and those for R and EW are always smaller than for the high ratio photospheric UV fluxes. The ratios for the chromospheric EW data agree well with those for the Mg II h & k lines in Figures 5.3 and 5.4 but differ significantly in Figures 5.5 - 5.7; however, the median and mean EW values agree well with the chromospheric Mg II and Si II + Al I continuum results in Figure 5.9 and 5.10, respectively. The poor match in 81-82, 82-83, and 83-84 provides a warning that we can not rely on the 1083 nm EW data to accurately represent the short-term variations of the solar UV flux for all time intervals. On the otherhand, it is much better than F10 for estimating the short-term UV variations.

5.5 Low Ratio for Si II Emission Lines

The point marked "Si II + Al I continuum" corresponds to just the first two terms in equation 8 at the end of Chapter 1. It includes variations from both the Al I continuum and two unresolved Si II emission lines The point marked "Si II with Al I cont. removed" corresponds to the revised flux in the Si II emission lines based on equation 8. In each of Figures 5.3 - 5.10, the power ratio for the Si II lines with the Al I continuum removed is distinctly lower than for the Si II lines together with the Al I continuum, and that in turn is distinctly lower than the ratio for 180 - 185 nm, which is also lower than the power ratio for the downward pointing triangle at 183 nm - just longward of the wavelengths affected by the Si II lines. This latter value agrees well with the ratios in the 195 - 210 nm range, which suggests that the chromospheric Si II lines near 182 nm, together with another Si II line near 181 nm, cause the ratio for the 180 - 185 nm band to be lower than the ratios for adjacent 5-nm bands.

5.6 Medium and Uniform Ratios for the Mg II Lines

In Figures 5.3 - 5.10, the 13- to 27-day power ratio for the center-to-wing ratio is slightly less than that for the flux at the center of the line. For all practical purposes, they are equal in their short-term variations. This means that the center-to-wing ratio, which is insensitive to instrumentation drift and is a good measure of long-term variations, is also a good measure of the short-term variations in the Mg II line. Much of the variation in the Mg II h & k lines occurs in the chromosphere despite the fact that much of the UV flux within the 1.1 nm bandpass of the NIMBUS-7 instrument originates in the upper photosphere even when centered on the combined h & k lines. Note that the median and mean ratios for the chromospheric He I equivalent width in Table 5.1 are close to those of the Mg II UV results. Also, it was

shown in Section 5.3 that the chromospheric EUV ratios agree well with the MG II h & k line ratio. In summary, we find the short-term temporal variations of the Mg II center-to-wing ratio to agree well with those of most other chromospheric fluxes. On the other hand, the 13- to 27-day power ratio for the Mg II h & k lines is always distinctly lower than for the photospheric UV fluxes in the 170 - 260 nm range and in the Mg I line at 285 nm.

Gao (1987) found a high correlation (r = 0.95 for Ca K 1A index, r = 0.97 for Ca-K K3) between mountain top measurements of the chromospheric Ca-K line of White et al. (1987) with the Mg II center-to-wing ratio for the long-term variations over solar cycle 21. For short-term variations, we have the NIMBUS-7 measurements of the Ca H & K lines, where the 1.1 nm bandpass does not fit these separate lines as well as for the Mg II overlapping lines and the results are noisy and sensitive to wavelength jitter in the instrument. The 13- to 27-day power ratios for the Ca H & K lines are 0.79 and 0.82, respectively, for the 205 nm normalized medians, which correspond to the other UV results shown in Figure 5.9, and 0.81 and 0.94 for the means corresponding to the other UV results in Figure 5.10. These results are closer to the photospheric results in the 170 - 260 nm range and the Mg I line than to the chromospheric Mg II results. We suggest this difference is a consequence of the NIMBUS-7 bandpass being larger relative to the separate Ca H and K lines than for the overlapping Mg II h & k lines and to greater limb darkening in the Ca data than in Mg II (Fredga, 1971).

5.7 Very High Ratios for the Al I Edge Ratio

In Figures 5.3 - 5.10, the 13- to 27-day power ratio for the Al I edge ratio is very high and quite variable (from 1.3 to 2.1 x the 205 nm ratio) with respect to the ratios in the UV fluxes responsible for inducing changes in the stratosphere, i. e. the 170 - 260 nm range. In most of these cases, the value is off the range of the figure and its true location is indicated by a small number marked below it. This is consistent with the time graphs for the Al I absorption-edge ratio differing from those of the UV fluxes in Chapter 2 and the autocorrelation functions for the edge ratio tending to have minor peaks near odd integer multiples of 14 days in Chapter 3. Apparently the head of the absoption edge at 208.8 nm is very rich in 13-day periodicity relative to the tail of the Mg I continuum absorption at 211.4 nm. The 5 nm bin results are usually slightly higher in the 195 - 210 nm range than in the 210 - 260 nm range and the edge ratio is an extreme example of this difference.

6. COMPLEX DEMODULATION ANALYSES

The complex demodulation analysis technique used here has been discussed in Chapters 4 - 7 of Heath et al. (1984) and by Lean and Repoff (1987). This analysis evaluates the amplitude and phase in the local vicinity of time t of the sinusoidal signal within the data at a selected reference frequency or period. The reference periods used here correspond to the peaks of the power spectra for the two main solar-rotation induced lines in the power spectra in Figures 5.1 and 5.2, namely about 27.7 and 13.4 days. Bouwer (1983) and Harvey (1984) showed that the frequency of greatest sinusoidal power varies slightly with time and from one episode to another. We have not fine tuned the period here to obtain the best one for each episode, but have used values that are a good average fit over the six years of NIMBUS-7 observations.

Figure 6.1 shows the amplitude of the complex demodulation function with respect to time over the six years studied. For each of these curves, a peak in the curve indicates strong 27-day sinusoidal variations in the vicinity of that time, where the main peaks occurred late in 1979, mid 1980, the end of 1981 through the start of 1982, and mid 1982, which can also be seen in the time graphs of Chapter 2. The main conclusion evident in Figure 6.1 is that **at UV wavelengths there is great uniformity in the 27-day variations** as they wax and wane. This means that the temporal variations at one UV wavelength combined with the relative amplitude function given in Figure 1.2 can closely estimate the 27-day variations in the 160 - 285 nm range.

Comparisons of the complex demodulation amplitude for the 205 nm UV flux have been made with respect to those for EUV flux measurements and various ground-based measures of solar activity and presented elsewhere; namely: modeled UV fluxes based on Ca-K plage data (Fig. 5, Lean et al., 1984); the sunspot number, 10.7 cm solar radio flux, and the equivalent width for the He I absorption line at 1083 nm (Fig. 5, Donnelly et al., 1985); and EUV fluxes (Donnelly et al., 1986a,b). Similarity occurred in the comparisons with the chromospheric 1083 nm data and the chromospheric EUV fluxes (H Lyman beta, He I 584 A, etc.). These were at most similar results, and not close to the great uniformity evident in Figure 6.1.

Figure 6.2 shows results for 205 nm for both of the main solar-rotation periodicities. The 205 nm flux has been found in Chapters 3 - 5 to be very representative of the temporal characteristics of the 170 -260 nm UV flux. In 1979 and 1980, when the 13-day periodicity was strong, the 27-day periodicity was weak, and vice versa (Donnelly et al., 1985). In 1981 - 1984, a mixture of these periodicities occurred rather than such separate episodes; however, the 13-day periodicity did not then rise and fall in phase lock with the 27-day periodicity. The 13-day periodicity is not a phase related harmonic of the 27-day variations; it is caused mostly by two peaks per solar rotation rather than being a harmonic of a highly nonsinusoidaly shaped 27-day variation. Figure 6.3 shows similar results for the photospheric Mg I line. Comparing Figures 6.2 and 6.3, the 27-day results are very similar and some minor differences are more evident for the 13-day periodicity.

Figure 6.4 compares the results for the UV flux at the center of the Mg II h & k lines combined with those for the center-to-wing ratio, i. e. Heath's UV index (UV1). These are a close match. On the otherhand, there are more differences between the curves in Figure 6.4 and the curves in Figures 6.1 - 6.3, especially for the 13-day periodicity, than there are among 6.1 - 6.3.

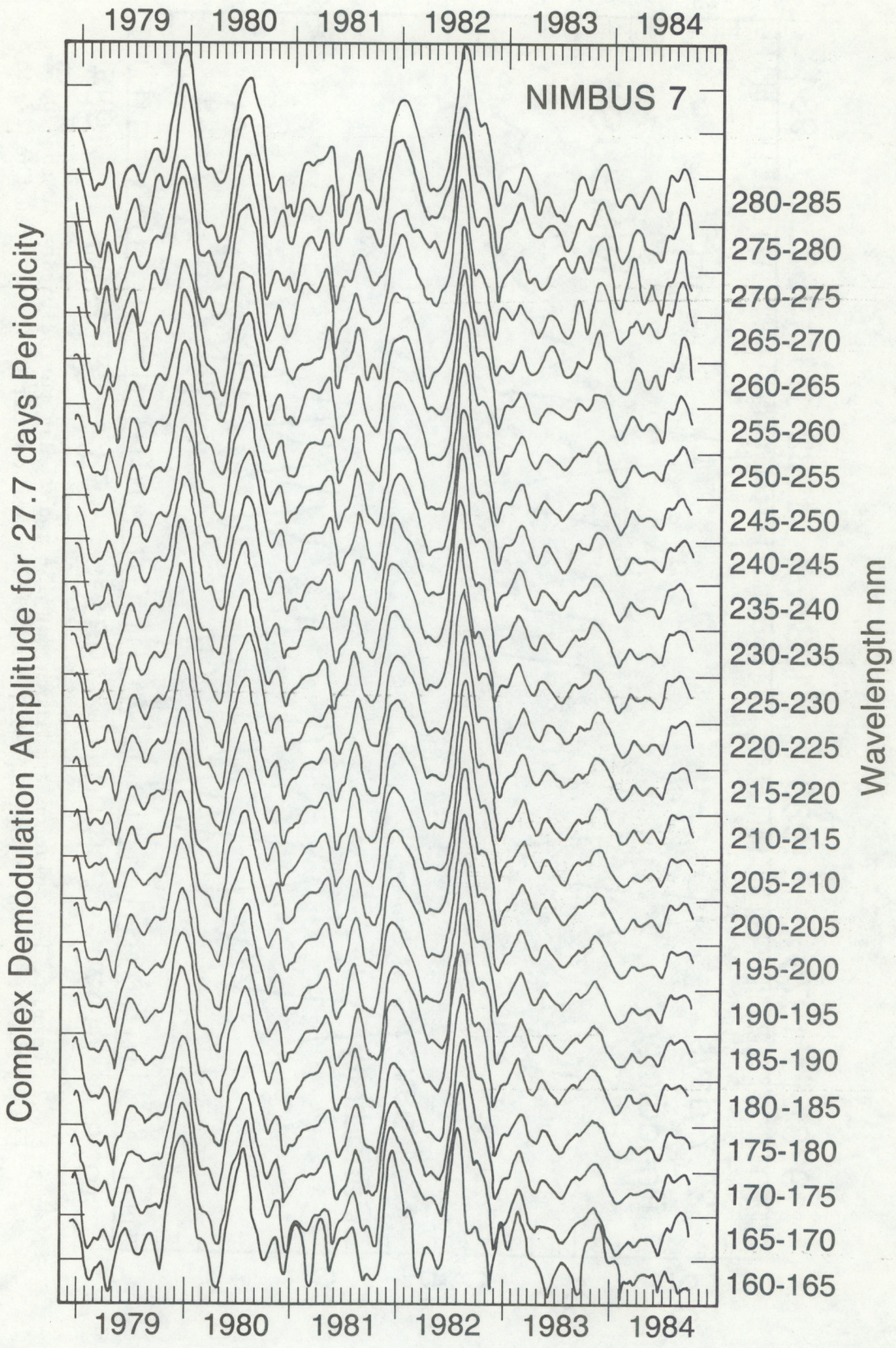

Figure 6.1 High uniformity in the temporal shape of the 27-day complex demodulation amplitude for UV wavelengths in the 160 - 285 nm range.

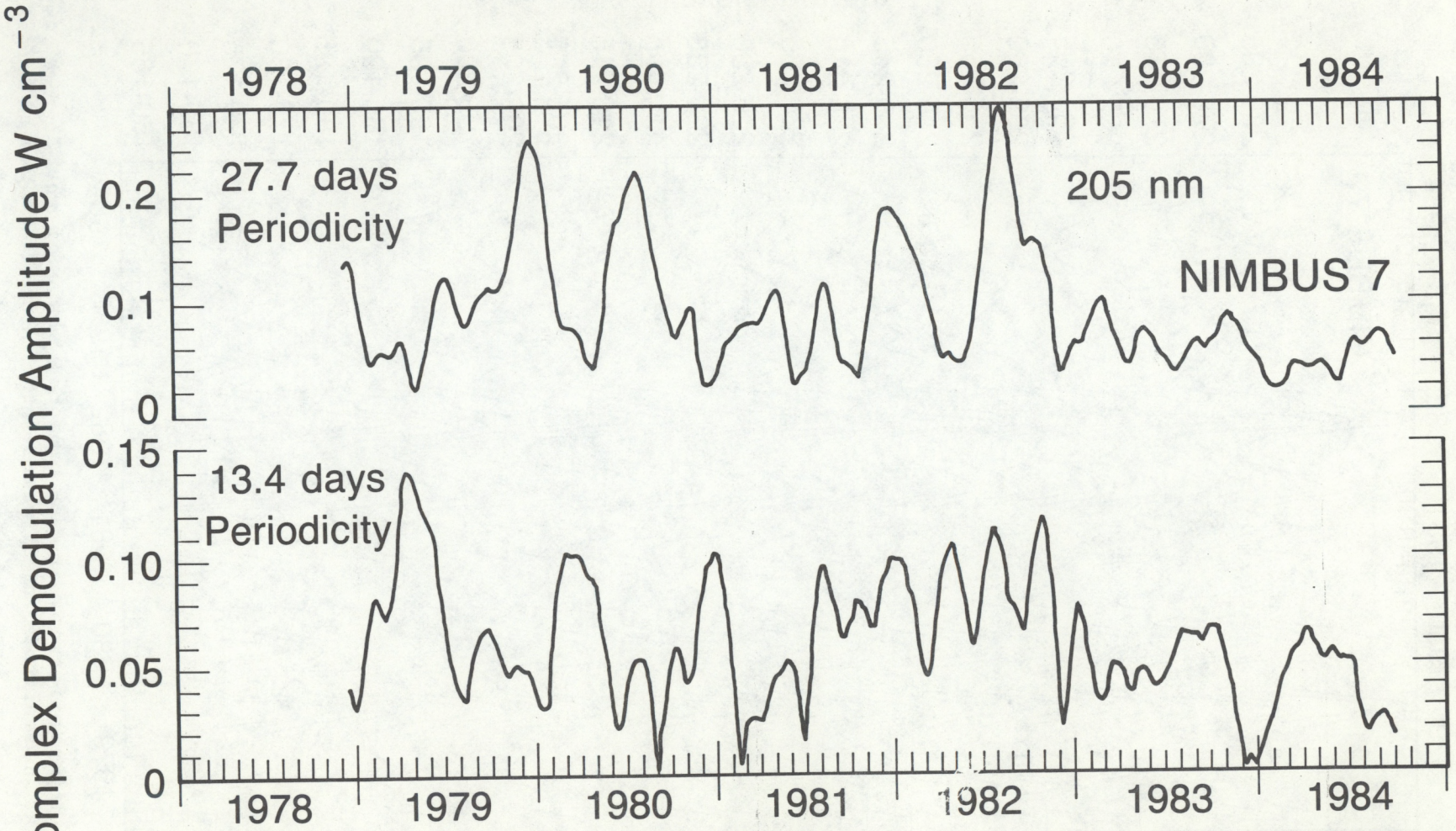

Figure 6.2 Complex demodulation amplitude for 13- and 27-day periodicities in the 205 nm flux. Note that in 1979 and 1980, the 13-day periodicity is low when the 27-day periodicity is large and vice versa.

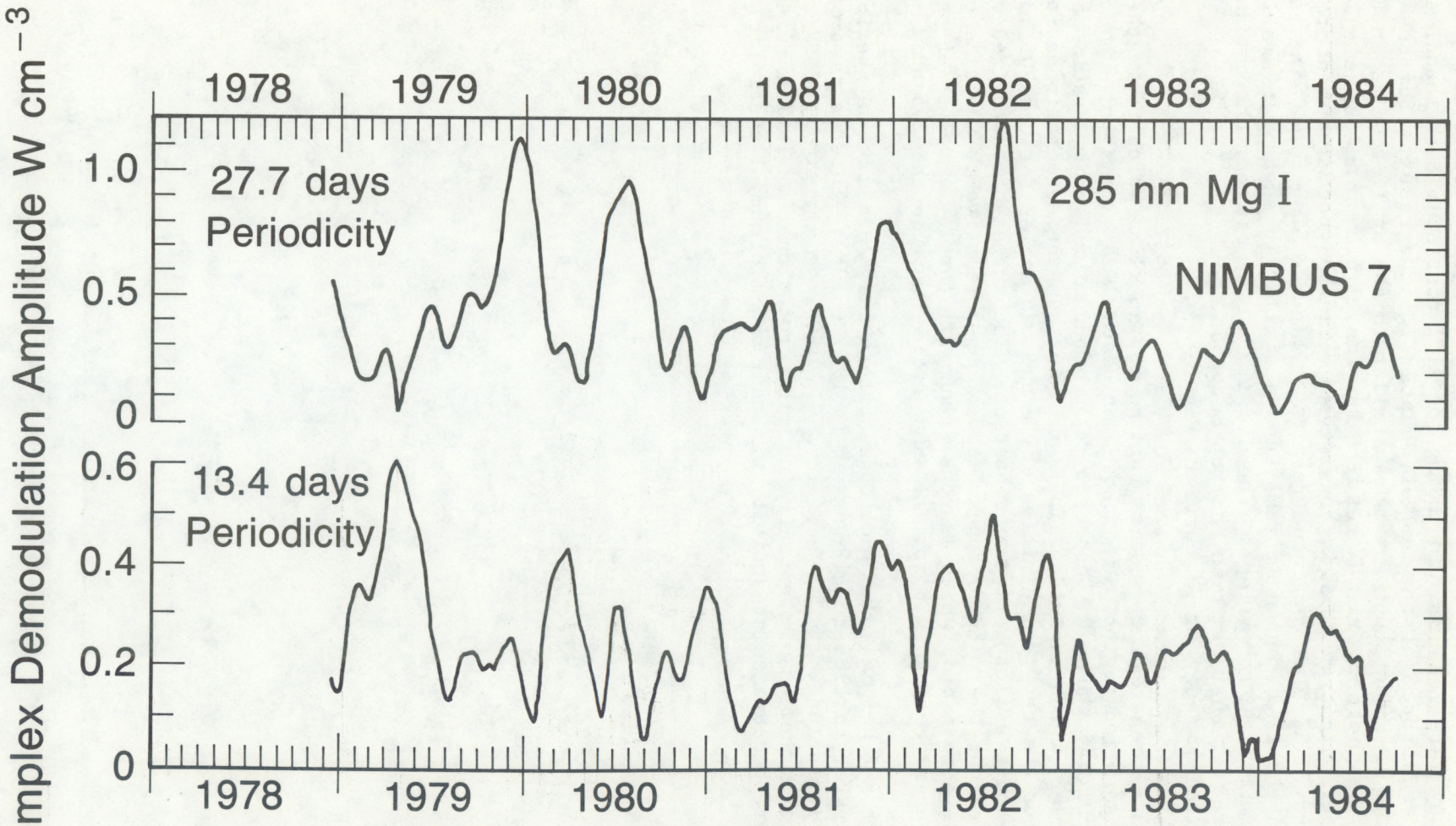

Figure 6.3 Complex demodulation amplitude for 13- and 27-day periodicities in the Mg I solar absorption line near 285 nm.

Figure 6.5 shows the complex demodulation analysis results for the Si II lines, as they were measured, including the Al I continuum background, and as revised by equation 8 at the end of Chapter 1. The results for the Si II lines plus the Al I continuum are more similar to the Mg II results in Figure 6.4 than to the photospheric UV results in Figures 6.1 - 6.3, especially for the 13-day periodicity. This is consistent with the good agreement between the Mg II and Si II plus continuum results in Figures 5.3 - 5.10. The revised results with the Al I continuum removed are similar in shape but smaller in amplitude, with deeper valleys. The dissimilarity between the bottom two curves is greater than between the top curve of these two (Si II with continuum) and the 13.4-day Mg II curve in Figure 6.4.

Figure 6.6 compares the results for the 205 nm flux, which is in the Al I continuum absorption region, with those for Heath's Al I continuum edge ratio. The edge ratio was shown in Chapter 5 to have anomolously high ratios of 13- to 27-day power, which is evident in Figure 6.6 from the edge ratio having the same scale for the two periodicities while the two scales for the 205 nm flux results are about a factor of two different. The shapes of the paired curves are similar except the valleys appear to be deeper relative to the size of the peaks for the edge ratio, which is consistent with the lower values of persistence in Figures 3.15 and 3.16 for the edge ratio than for the 205 nm flux.

In Figures 6.1 - 6.1, the amplitude of both the 27- and 13-day periodicities are smaller in 1983 and 1984 than in 1979 - 1983. This is part of the solar cycle variation of solar activity. In 1986, in the NOAA-9 SBUV/2 data not shown here, there is essentially no solar rotational variation in August and September, because solar activity was near the minimum of the solar cycle.

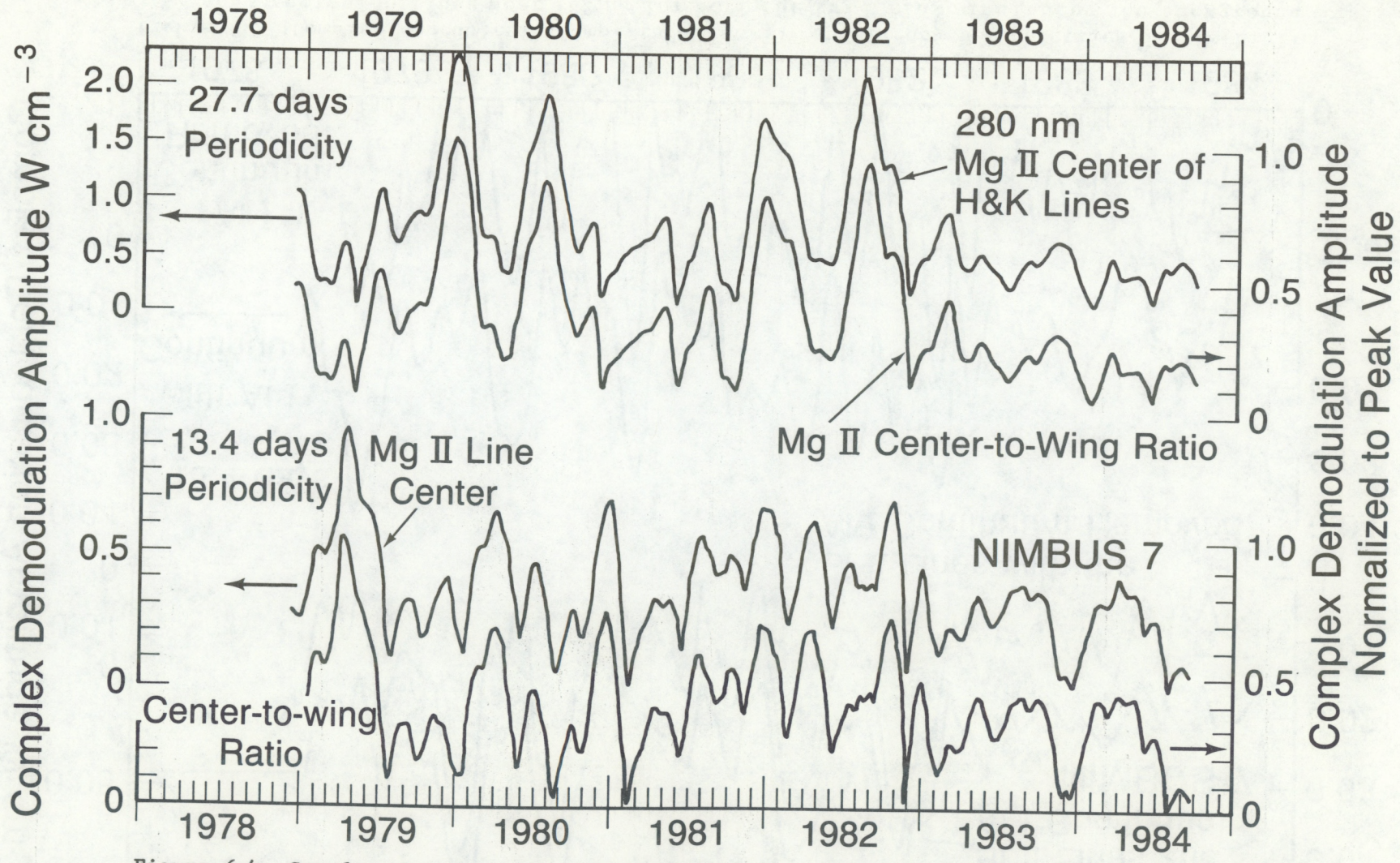

Figure 6.4 Complex demodulation amplitude for 13- and 27-day periodicities in the Mg II solar absorption lines near 280 nm for both the center-of-line flux and the center-to-wing ratio.

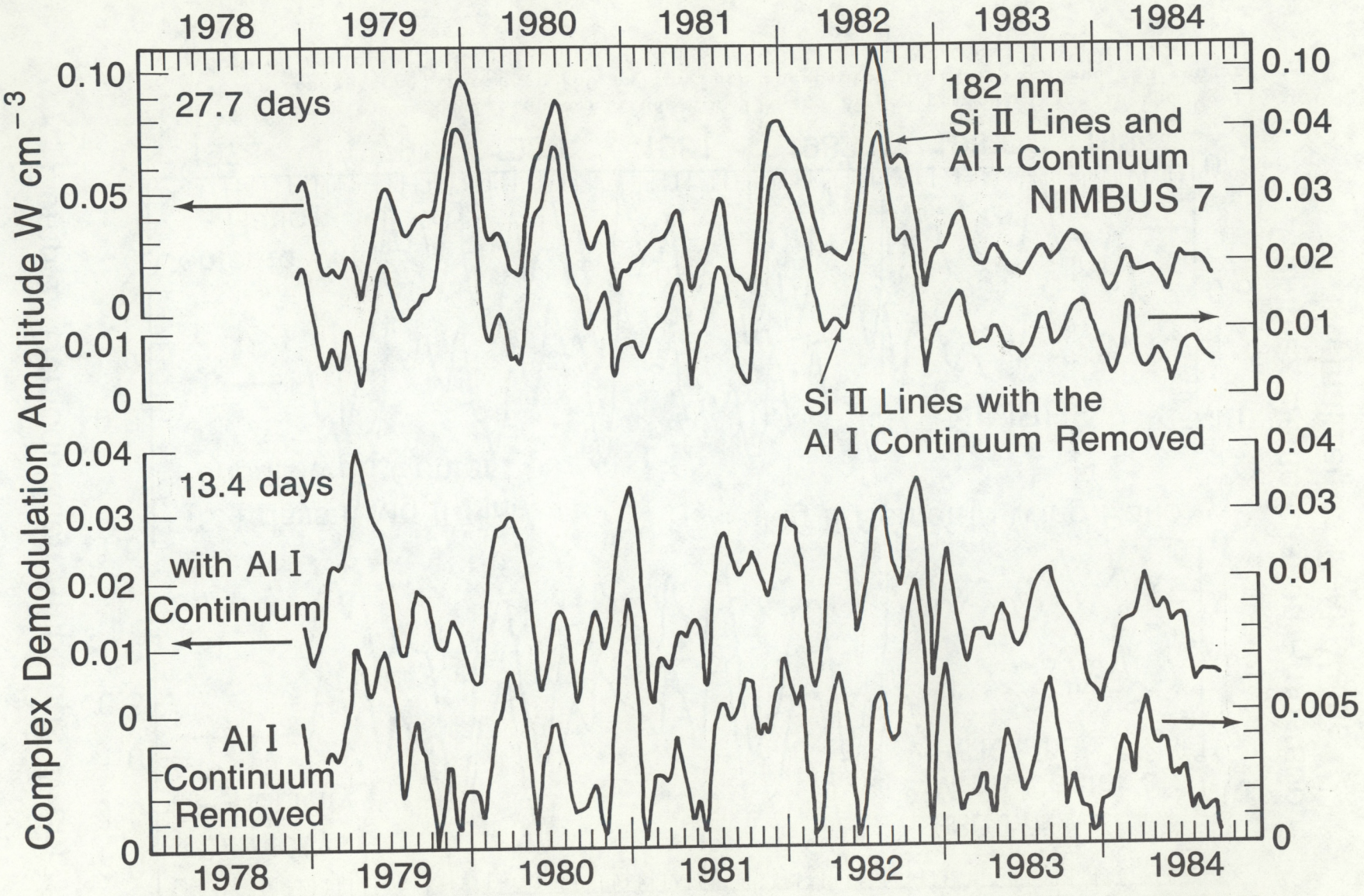

Figure 6.5 Complex demodulation amplitude for 13- and 27-day periodicities in the Si II solar emission lines near 182 nm for both the full flux, including the background continuum, and the line with an estimate of the background continuum removed.

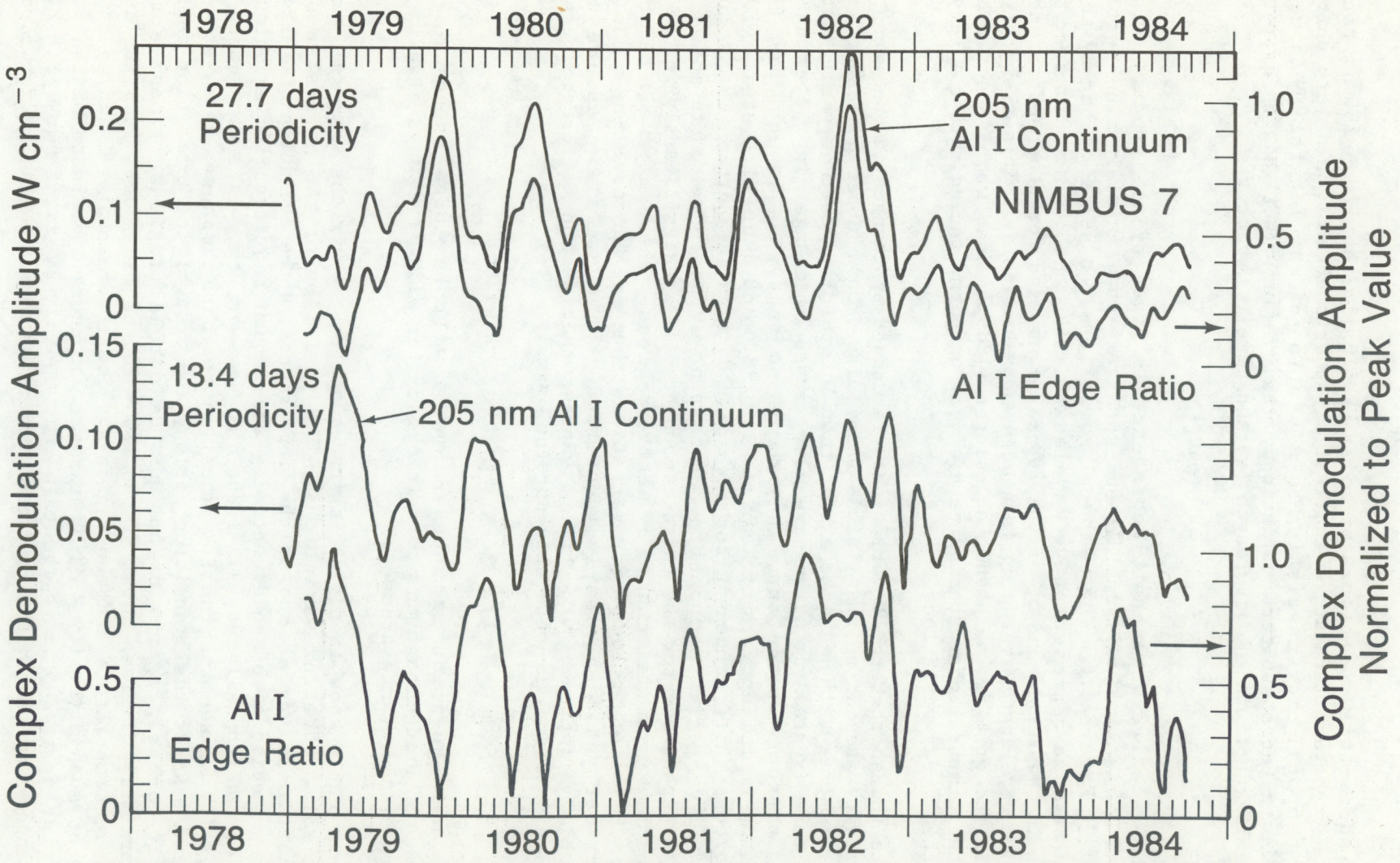

Figure 6.6 Complex demodulation amplitude for 13- and 27-day periodicities in both the 205 nm flux in the Al I absorption continuum and the Al I edge ratio.

7. DISCUSSION

The short-term variations of solar UV flux in the 170 - 260 nm range, which are important because of their stratospheric effects, are very uniform in their temporal characteristics as a function of wavelength. This means that at least for short-term variations, the UV flux F(w,t) can be expressed as separable functions of wavelength (w) and time (t), namely:

$$F(w,t) = W(w)V(t), \tag{12}$$

where the relative wavelength dependence is given by the product of the fractional variation in Figure 1.2 and some reference initial-value UV flux, like that in Figure 1.1. The temporal variations can be described by those measured at some representative wavelength, like the 205 nm flux used as a reference in Chapters 3 and 5, or the 200 - 205 nm band for other measurements where some wavelength averaging is needed to reduce noise. This viewpoint is evident in the work of Heath and Schlesinger (1986). What we have shown here is that the temporal characteristics are very uniform, including the 13-day as well as the 27-day variations.

Since the short-term UV variations are caused by changes in the amount of solar activity present on the visible solar disk in the upper photosphere and lower chromosphere, then to the extent that intermediate-term (several months) and long-term (years) variations are also caused by changes in the amount of activity present on the sun, they may also behave as in equation (12). Although the modeling work of Lean et al. (1982) and Skumanich et al. (1984) have invoked a third component for the solar UV flux in addition to the quiet sun and active-region components, we have no evidence yet that shows the wavelength dependence for the third component differs significantly in the 170 - 260 nm range from that caused by active regions. There may well be other processes involved in long-term variations that are inconsistent with (12) that have not yet been clearly identified. However, if we assume such nonseparable variations (N) occur and express them as the difference between the total flux F and the separable portion, namely:

$$N(w,t) = F(w,t) - W(w)V(t), \tag{13}$$

then the main question is whether N(w,t) will be large enough or the measurements good enough to prove it exists, or will it always hide in the error bars of the UV measurements?

We currently know that (12) is inadequate to explain the temporal variations of solar EUV flux variations. The variation of the persistence of solar-rotational variations or the differences in the evolution of emission during major episodes of solar activity are enough to disqualify equation 12 for EUV fluxes (Donnelly et al., 1986a,b). However, this is a consequence of different EUV fluxes originating in either the chromosphere, upper chromosphere plus base of the transition region, the rest of the transition region, old "cool" coronal regions or hot active coronal regions. These source regions are very diverse. Most of the 170 - 260 nm flux comes from the upper photosphere, temperature minimum region and lower chromosphere, and we do not yet know of much diversity in this range. Our current estimate of the solar cycle variation at 205 nm is about 10% for monthly averages for cycle 21, a small change compared to the couple of orders of magnitude change for coronal EUV fluxes.

Heath's solar UV1 index, the Mg II center-to-wing ratio (Heath and Schlesinger, 1986), is very important because it is fairly insensitive to drifts in instrumentation and is therefore useful for long-term measurements. We included it in our studies of short-term variations here to see if it is also a good candidate for determining the short-term temporal dependence (V) for the UV fluxes in the 170 - 260 nm range. UV1 agrees well for 27-day variations but is definitely weaker in 13-day variations. Modeling of the short-term UV flux variations by Puga et al. (1987, Section 2.4) shows that the difference between the Mg II and other UV ratios of 13- to 27-day power can be explained as a difference in their center-to-limb variations of plage emission, where the lower ratio fits with a less rapid decline in plage emission with increasing solar central angle for plages near the solar limb for the chromospheric Mg II h & k lines than for the other more photospheric UV flux variations. This less rapid decline in plage emission makes sense for chromospheric fluxes because of their higher altitude in the solar atmosphere. This interpretation means that it is primarily the amplitude of the 13-day variations that differ in the Mg II and 170 - 260 nm data, with smaller 13-day amplitudes in the Mg II data than in the other UV data because the plage emission is relatively stronger for the Mg II lines when the two groups of active regions are each near one of the solar limbs, which decreases the depth of the local minima for 13-day variations. For 27-day variations, the amplitudes are not affected, just the temporal width of the peak is slightly narrower for photospheric UV flux variations compared to those for the chromospheric Mg II lines.

The lower strength of 13-day variations in UV1 makes sense in terms of the chromospheric source of the cores of the h & k lines and the upper photosphere and lower chromosphere source for most of the flux in the 170 - 260 nm range. Because of the uniformity of the 13-day/27-day periodicty for Heath's UV index relative to that for 170 - 260 nm, it would, in principle, be possible to use the Mg II ratio to estimate the short-term 170 - 260 nm variations, as well as long-term variations, and to include corrections for 13-day variations. A more practical solution is to use the 205 nm flux (or 200 - 205 nm band) to represent the short-term variations and the Mg II center-to-wing ratio for intermediate- and long-term variations, since this does not require any corrections for the 13-day variations.

The Al I edge ratio (UV2), a second measure appropriate for long-term variations, does not match the short-term variations in the 170 - 260 nm range as well as the Mg II center-to-wing ratio does. UV2 is noisier, lower in persistence of the solar-rotational modulation, and much stronger in 13-day periodicity. Therefore, we do not consider the Al I edge ratio as useful for estimating the short-term variations of the UV flux that is important to the stratosphere. On the other hand, we do consider it useful for intercomparing the long-term variations from different satellites to try to detect differences in their instruments.

Heath and Schlesinger (1986) used the Mg II center-to-wing ratio together with the wavelength dependence of short-term UV variations to derive the long-term UV variations at other wavelengths. They used a linear regression analysis of the 27-day minimum to peak variations to derive the factor that when multiplied by the Mg II flux would give the expected Al I edge ratio values. They then compared the UV1 estimated Al I ratio with the value derived from the NIMBUS-7 measurements and showed the residuals had little or no long-term variation, i. e. the estimated and observed values tracked each other, over

the long term. Our analysis shows that the 13-day variations are low in UV1 and high in UV2. Because Heath and Schlesinger's regression analysis was based on 27-day variations and happened to exclude 13-day variations, they avoided problems that might otherwise have been introduced by the 13-day variations. We conclude that their regression analysis was very good and agree that their Al I ratio test suggests that equation 12 is at least suitable for the UV flux near 210 nm for long-term variations. We also conclude that the short-term residuals in the top of their Figure 6 are rich in 13-day variations. The ratio of 13-day to 27-day power for UV2 divided by the corresponding ratio for UV1 for the results in Figures 5.3 - 5.7 range from 2.6 to 4.5, with a median value of 3.27 and mean of 3.26. That large difference from unity would contribute much of their short-term residuals.

The anomolous 13- to 27-day power ratio for the Al I continuum edge should be studied further by studying the 13- to 27-day power ratio for the short-term variations of F(w1)/F(w2), with w1 and w2 taking on values that are equal steps away from the center of the edge and in opposite directions. This would be of interest from a solar physics viewpoint. It may also be possible to pick slightly different wavelengths to obtain an Al I edge ratio that is less anomolous in its short-term variations.

Although the Mg II center-to-wing ratio does not match the 13-day variations of the 170 - 260 nm UV flux, it does compare nicely with the chromospheric EUV flux variations (Donnelly et al., 1986a,b), and may be useful for estimating their temporal variations. On the other hand, the 13-day to 27-day power ratio for the chromospheric Si II line with the background Al I continuum removed is much lower than for other chromospheric measures, like the Mg II h & k lines and the 1083 nm equivalent width. Among the EUV results, the power ratio for H Lyman alpha was also anomalously low (Donnelly et al., 1986b). These two low cases serve as a warning that we should not assume the 13- to 27- day periodicity is fairly constant with respect to wavelength for all chromospheric emissions. Different chromospheric emissions can have different center-to-limb functions, which is what mainly determines the strength of the 13-day periodicity. This, combined with the decrease in 13- to 27- day periodicity in Figures 5.3 - 5.10 with decreasing wavelength from the 175 - 180 nm band to the 160 - 165 nm band (which we conclude is the consequence of the increasing influence of chromospheric emission lines), suggests that the SME measurements of UV flux in the 120 to 180 nm range will probably show low 13-day periodicity. This means that the UV radiation that affects the mesosphere should have weaker 13-day periodicity than the UV flux that affects the stratosphere.

8. CONCLUSIONS

1. Short-term temporal variations in the solar UV flux are highly uniform in their relative temporal characteristics as a function of wavelength in the 170 - 260 nm band and the Mg I line at 285 nm, especially compared to the great diversity of temporal characteristics seen in EUV fluxes and ground-based measures of solar activity. Therefore, the UV radiation variations that induce changes in the stratosphere are highly uniform in their relative temporal characteristics, where "relative" refers to the fact the amplitude of these variations does vary with wavelength as indicated in Figure 1.2. This uniformity was shown to occur for 27-day and 13-day solar-rotation induced variations in Chapter 6, for the relative strength of 13 to 27 day power in Chapter 5, for the cross correlation with respect to the UV flux at the representative wavelength of 205 nm in Chapter 4, and for the persistence of solar-rotational variations during the evolution of major episodes of solar activity in Chapter 2. This uniformity means that short-term variations of the UV flux may be expressed in terms of separable functions of wavelength and time, as discussed in Chapter 7.

2. We recommend that the 205 nm flux (or the 200 - 205 nm flux for data that requires wavelength averaging to reduce noise) be used to determine the time function for short-term variations. Although we accept Heath and Schlesinger's (1986) Mg II center-to-wing ratio (UV1) as the best available indicator of long-term temporal variations, we do not recommend it for short-term variations because it is not as strong in 13-day variations as the 170 - 260 nm flux. While we accept the Al I edge ratio (UV2) as a good measure of long-term UV variations for use in comparing data from two different satellites to try to detect differences in their instruments, we find it is too noisy and too strong in 13-day periodicity to represent the short-term variations in the 170 - 260 nm range. The differences found in the short-term variations of UV1 or UV2 relative to the 170 - 260 nm flux do not affect the results of Heath and Schlesinger (1986), they only help explain some of their short-term residuals.

3. The UV flux variations were rich in 13-day variations as well as the very strong 27-day variations throughout the six years of data studied. While in 1979 and 1980, the episodes of strong 13-day periodicity were essentially separate from those of strong 27-day variations; in 1981 - 1984, a more complicated mixture of 13- and 27-day variations occurred. Most of the power in 13-day variations comes from two peaks per solar rotation rather than from a phase related harmonic of a 27-day fundamental with a highly nonsinusoidal shape. The photospheric UV fluxes are stronger in 13-day variations relative to their 27-day variations than any other solar data we have studied, which includes EUV fluxes and various ground-based measures of solar activity. Chromospheric UV fluxes, like the Si II lines near 182 nm and the Mg II h & k lines, did not have quite as strong of 13-day variations as did the more photospheric UV fluxes.

4. The persistence of solar-rotational modulation is very high for photospheric UV fluxes, like those in the 170 - 260 nm range, again, higher than for any other solar data we have studied. These highly sinusoidal variations with both 13- and 27-day periods and sometimes with marked phase shifts from one major episode to another should be beneficial characteristics to help unravel the physics of the stratospheric effects of these UV flux variations.

REFERENCES

Banks, P. M., and G. Kockarts, Aeronomy, Academic Press, New York, 1973.

Bouwer, S. D., Intermediate-term epochs in solar soft X ray emission, J. Geophys. Res., 88, 7823-7830, 1983.

Donnelly, R. F., D. F. Heath and J. L. Lean, Active-region evolution and solar rotation variations in solar UV irradiance, total solar irradiance, and soft X rays, J. Geophys. Res., 87, 10318-10324, 1982.

Donnelly, R. F., D. F. Heath, J. L. Lean and G. J. Rottman, Differences in the temporal variations of solar UV flux, 10.7-cm solar radio flux, sunspot number, and Ca-K plage data caused by solar rotation and active region evolution, J. Geophys. Res., 88, 9883, 1983.

Donnelly, R. F., D. F. Heath, J. L. Lean and G. J. Rottman, Temporal variations of solar UV spectral irradiance caused by solar rotation and active region evolution, Solar Irradiance Variations on Active Region Time Scales, NASA Conf. Publ. 2310, Eds. B. J. LaBonte et al., Sci. Tech. Info. Branch, NASA, Washington, D. C. 20546, 233 - 249, 1984.

Donnelly, R. F., H. E. Hinteregger and D. F. Heath, Temporal variations of solar EUV, UV and 10830-A Radiations, J. Geophys. Res., 91, 5567-5578, 1986a.

Donnelly, R. F., J. W. Harvey, D. F. Heath and T. P. Repoff, Temporal characteristics of the solar UV flux and He I Line at 1083 nm, J. Geophys. Res., 90, 6267 - 6273, 1985.

Donnelly, R. F., L. C. Puga, and W. S. Busby, Temporal characteristics of solar EUV, UV and 10830-A full-disk fluxes, NOAA Tech. Memo. ERL ARL-146, NOAA ERL, Boulder, Colo., 127 pp, 1986b.

Donnelly, R. F., Solar UV spectral irradiance variations, Weather and Climate Responses to Solar Variations, ed. B. M. McCormac, pp. 43 - 55, 1983.

Donnelly, R. F., Temporal trends of solar EUV and UV full-disk fluxes, accepted for publication in Solar Phys., 1987.

Fredga, K., A comparison between Mg II and Ca II spectroheliograms, Solar Phys., 21, 60-81, 1971.

Gao, M., Comparison of full-disk Ca-K line measurements and NIMBUS-7 UV flux measurements, section 3.8 in Puga et al. (1987).

Hanson, K. J., Monitoring the Solar Constant and Solar Ultraviolet, Report and Recommendations from a Workshop Held at Estes Park, Colorado, 8-12 August 1977, 70 pp., Air Resources Labs., NOAA ERL, Boulder, Colorado, 1978.

Harvey, J., Helium 10830A irradiance: 1975-1983, Solar Irradiance Variations on Active Region Time Scales, NASA Conference Publ. 2310, eds. B. J. LaBonte et al., 197 - 211, 1984.

Heath, D. F., A. J. Krueger, H. A. Roeder and B. D. Henderson, The solar

backscatter ultraviolet and total ozone mapping spectrometer (SBUV/TOMS) for NIMBUS G, Optical Eng., 14, 323 - 331, 1975.

Heath,D. F., and B. M. Schlesinger, J. Geophys. Res. **91**, 8672, 1986.

Heath, D. F., A review of observational evidence for short and long term ultraviolet flux variability of the sun, Sun and Climate, Centre National D'Etudes Spatiales, 18 Avenue Edouard - Belin, 31055 Toulouse Cedex, France, 447-471, 1980.

Heath, D. F., T. P. Repoff and R. F. Donnelly, NIMBUS-7 Observations of Solar UV Spectral Irradiance Variations Caused by Solar Rotation and Active-Region Evolution for the Period November 7, 1978 - November 1, 1980, NOAA Tech. Memo. ERL ARL-129, Air Resour. Lab., Environ. Res. Lab., Natl. Oceanic and Atmos. Admin., Boulder, Colo., 75 pp., 1984.

Lean, J. L., T. P Repoff and D. F. Heath, Statistical comparison of observed and modelled solar UV irradiance variations with solar activity parameters during the maximum of solar cycle 21, IRS '84: Current Problems in Atmospheric Radiation, ed. G. Fiocco, A. Deepak Publ., Sci. & Tech. Corp., Hampton, Virginia, U. S. A., 325 - 328, 1984.

Lean, J. L., and T. P. Repoff, A statistical analysis of solar flux variations over time scales of solar rotations: 1978-1982, J. Geophys. Res., 92, 5555 - 5563, 1987.

Lean, J. L., O. R. White, W. C. Livingston, D. F. Heath, R. F. Donnelly, and A. Skumanich, A three-component model of the variability of the solar ultraviolet flux: 145-200 nM, J. Geophys. Res., 87, 10307-10317, 1982.

Puga, L. C., R. F. Donnelly, J. Barrett, K. Pfendt, D. Stevens, and M. Gao, The NOAA-ERL-ARL Solar UV Radiation and Climate Research Project, Program Description and Progress Report, to be published as a NOAA Tech. Memo., 1987.

Skumanich, A., J. L. Lean, O. R. White and W. C. Livingston, The sun as a star: three-component analysis of chromospheric variability in the calcium K line, Astrophys. J., 282, 776-783, 1984.

White, O. R., W. C. Livingston and L. Wallace, Variability of chromospheric and photospheric lines in solar cycle 21, J. Geophys. Res., 92, 823 - 827, 1987.